ORIGINAL ARTICLE

A role of the Trx-G complex in Cid/CENP-A deposition at *Drosophila melanogaster* centromeres

Lucia Piacentini[1] · Marcella Marchetti[1] · Elisabetta Bucciarelli[2] · Assunta Maria Casale[1] · Ugo Cappucci[1] · Paolo Bonifazi[1] · Fioranna Renda[1,3] · Laura Fanti[1]

Abstract
Centromeres are epigenetically determined chromatin structures that specify the assembly site of the kinetochore, the multiprotein machinery that binds microtubules and mediates chromosome segregation during mitosis and meiosis. The centromeric protein A (CENP-A) and its *Drosophila* orthologue centromere identifier (Cid) are H3 histone variants that replace the canonical H3 histone in centromeric nucleosomes of eukaryotes. CENP-A/Cid is required for recruitment of other centromere and kinetochore proteins and its deficiency disrupts chromosome segregation. Despite the many components that are known to cooperate in centromere function, the complete network of factors involved in CENP-A recruitment remains to be defined. In *Drosophila*, the Trx-G proteins localize along the heterochromatin with specific patterns and some of them localize to the centromeres of all chromosomes. Here, we show that the Trx, Ash1, and CBP proteins are required for the correct chromosome segregation and that Ash1 and CBP mediate for Cid/CENP-A recruitment at centromeres through post-translational histone modifications. We found that centromeric H3 histone is consistently acetylated in K27 by CBP and that *nej* and *ash1* silencing respectively causes a decrease in H3K27 acetylation and H3K4 methylation along with an impairment of Cid loading.

Keywords Centromere · CENP-A/Cid · Trx-G proteins · H3 histone modifications · Chromosome segregation · *Drosophila melanogaster*

Introduction

Centromeres are specialized chromatin structures that establish the assembly site for the kinetochore, a complex multilayered protein structure that mediates the attachment of spindle microtubules to chromosomes, thus permitting proper chromosome segregation during cell division. The centromeres of higher eukaryotes usually appear as primary constrictions along mitotic chromosomes and are located in heterochromatic regions that contain satellite DNA repeats. However, satellite sequences are neither necessary nor sufficient for centromeric function, as different chromosomal regions may acquire centromeric properties (Voullaire et al. 1993; du Sart et al. 1997; Amor et al. 2004; Warburton 2004; Fukagawa and Earnshaw 2014).

Increasing evidence indicates that protein composition has an important role in centromere specification and behavior (Warburton et al. 1997; Baum et al. 2006; Nakano et al. 2008; Muller and Almouzni 2017). Centromeric protein A (CENP-A) and its *Drosophila* orthologue centromere identifier (Cid) are H3 histone variants that replace canonical histone H3 in centromeric nucleosomes (Earnshaw and Rothfield 1985; Sullivan et al. 1994; Buchwitz et al. 1999). CENP-A/Cid deficiency disrupts chromosome segregation because this histone variant is required for recruitment of other centromere and kinetochore proteins, which form the constitutive centromere-associated network (CCAN) (Takahashi et al. 2000; Howman et al. 2000; Oegema et al. 2001; Blower and Karpen 2001; Régnier et al. 2005; McKinley and Cheeseman 2016).

✉ Laura Fanti
laura.fanti@uniroma1.it

[1] Istituto Pasteur Italia, Dipartimento di Biologia e Biotecnologie "Charles Darwin", Università "Sapienza", Rome, Italy

[2] Istituto di Biologia e Patologia Molecolari del CNR, Rome, Italy

[3] Present address: Wadsworth Center, New York State Department of Health, Albany, NY 12201, USA

The maintenance of centromere identity requires new CENP-A/Cid recruitment after centromeric DNA replication. This process occurs in different phases of the cell cycle, and it is usually uncoupled to DNA replication (De Rop et al. 2012; Chen and Mellone 2016). In human cells, CENP-A deposition occurs in late telophase or in early G1 (Jansen et al. 2007). In *Drosophila* early embryos, Cid is incorporated into the chromosomes during anaphase (Schuh et al. 2007), while in *Drosophila* Kc tissue culture cells, Cid recruitment occurs in G2 and metaphase (Ahmad and Henikoff 2001); in cultured S2 cells, the peak of CENP-A/Cid loading occurs in early G1 phase (Lidsky et al. 2013) although a transient increase of centromeric CENP-A/Cid was observed during mitotic metaphase (Mellone et al. 2011). There is also evidence that specific post-translational modifications play an important role in CENP-A/Cid deposition after DNA replication (Sullivan and Karpen 2004; Ekwall 2007; Molina et al. 2017).

The analysis of extended chromatin fibers has shown that blocks of CENP-A/Cid nucleosomes are linearly interspersed with nucleosomes containing canonical H3 histones in both human and *Drosophila* cells (Blower et al. 2002; Sullivan and Karpen 2004). The CENP-A N-terminal tail may undergo post-translational modifications like methylation, phosphorylation, acetylation, and ubiquitination (reviewed in Rošić and Ehardt 2016). In addition, centromeric H3 nucleosomes lack characteristic heterochromatin marks, such as di- and trimethylation of H3 at lysine 9; instead, they contain active chromatin marks such as di-methylation of H3 at lysine 4, but they are hypoacetylated (Sullivan and Karpen 2004). This combination of post-translational modifications within the heterochromatin is thought to delimit a region of open chromatin that would promote the CENP-A/Cid recruitment (Bernad et al. 2009).

In addition to CENP-A/Cid, many additional proteins have been identified with roles in the centromere function; mutations in genes encoding these proteins have been shown to cause defects in chromosome segregation (for review, see Przewloka and Glover 2009). However, the complete network of determinants and epigenetic marks involved in CENP-A/Cid recruitment remains to be defined. Polycomb group (Pc-G) and Trithorax group (Trx-G) proteins are highly conserved epigenetic factors (Kennison 1993) that regulate gene expression by controlling deposition and recognition of histone modifications and chromatin structure (reviewed in Geisler and Paro 2015). The Pc-G and Trx-G proteins are primarily involved in repressing and activating gene expression, respectively (Kennison 1993; Geisler and Paro 2015). However, the *Drosophila* Trx-G proteins not only are localized in euchromatin but are also enriched in heterochromatin with a specific and reproducible localization pattern (Fanti et al. 2008). Specifically, several Trx-G proteins localize at the centromeric regions of all chromosomes (Fanti et al. 2008). This finding prompted us to ask whether these proteins have roles in

centromere assembly and function. Here, we show that the Trx-G proteins Ash1 and CBP localize to the *Drosophila* centromeric regions and are required for correct CENP-A/Cid recruitment at centromeres and for chromosome segregation.

Materials and methods

Drosophila stocks and culture conditions

All the stocks used here were obtained from the Bloomington Stock Center. To define the functions of the *ash1* gene, we used the amorphic *ash1*^{06} and *ash1*^{22} lethal alleles. For the functional analysis of the CREB-binding protein (CBP)–encoding gene *nejire* (*nej*), we used the *nej* RNA interference (RNAi) line P{UAS-nej.siRNA}hp12, w* (BL #32576). Larvae bearing a P{UAS-nej.siRNA}hp12 construct and a heat shock–inducible GAL4 driver were reared at 25 °C until the second instar; then, they were grown at 29 °C for about 18 h and heat shocked at 37 °C for 1 h. For the *trithorax* (*trx*) gene, we used the amorphic *trx*^{B16} allele and the trx RNAi line y^1 sc* v^1 P {TRiP.HMS00580}attP2 (BL #33703); the elav-GAL4 driver (BL #458) was used for constitutive expression of trx RNAi transgenes in the nervous system; for the *Polycomb* (*Pc*) gene, we used the amorphic *Pc*^{1} allele. As a control, we used a Canton-S strain kept for many years in our laboratory. For a detailed description of these stocks, see FlyBase (http://flybase.bio.indiana.edu).

Flies were maintained at 24 °C on a standard *Drosophila* medium containing cornmeal, yeast, sucrose, agar, and propionic acid as a mold inhibitor.

Cytological analysis of mutant embryos

To prepare embryos for whole-mount immunofluorescent analysis, 2- to 4-h-old *Drosophila* embryos were collected, dechorionated in 50% bleach, and fixed in 1:1 (*v:v*) mix of 37% formaldehyde and heptane for 5 min. Embryos were devitellinized with 100% methanol as described in Rothwell and Sullivan (1999) and rehydrated with extensive rinse in 1X PBS. Propidium iodide was used to stain DNA. Before staining with propidium iodide, the embryos were incubated with RNase A, at a concentration of 10 μg/ml, at 37 °C for 2 h, to remove the RNA. Propidium iodide was added to the mounting medium at the final concentration of 1 μg/ml. Antibody staining was carried out overnight in PBTA (1X PBS, 1% BSA, and 0.05% Triton-X) at 4 °C. The antibodies used were mouse anti-tubulin (1:100, Sigma #T9026) and Cy^2-conjugated goat anti-mouse (1:50, GE Healthcare). Confocal images of fixed and stained embryos were acquired on an inverted Leica DM IRE2 microscope with a Leica TCS SP2 confocal laser scanner.

RNA interference

D. melanogaster S2 cells were cultured at 24 °C in Shields and Sang M3 medium (Sigma) supplemented with 10% heat-inactivated fetal bovine serum (FBS, Gibco).

dsRNAs against *ash1*, *nej*, *trx*, and *cid* were synthesized by in vitro transcription from PCR products with T7 promoters on both ends of the amplicons, using the Megascript RNAi kit (Ambion).

Off-target analysis was performed with dsCheck online search tool (http://dscheck.rnai.jp/) (Naito et al. 2005). While we can rule out the presence of off-targets for Cid, Ash1 and Trx, we have seen that there were some for CBP (nej). Therefore, we examined suitably immunostained extended chromatin fibers, mitotic chromosomes, and cells stably expressing SNAP-tagged Cid cells using also an independent couple of primers (nej 2) for the preparation of the double strand RNA of *nej*.

The T7-linked (TAATACGACTCACTATAGGGAGA) primers used in the PCR reactions were:

> *ash1* F 5′-GTGGACAAGACGG-3′
> *ash1* R 5′-CGGACAGCAGGTA-3′
> *nej* F 5′-AATGGCGGAAACA-3′
> *nej* R 5′-TTGGACTGATGCT-3′
> *nej* 2 F 5′-TATGAAACCTGGTGGCGGTC
> *nej* 2 R 5′-CGTTTGCATCACATGGGTGG
> *trx* F 5′-TGCGACCCTCCAT-3′
> *trx* R 5′-CCCTCTTCCAGCA-3′
> *cid* F 5′-TCGGCGAACAAC-3′
> *cid* R 5′-TCGGCGAACAAC-3′

1×10^6 cells were plated in 1 ml of serum-free medium in a well of a six-well culture dish (Sarstedt). Each culture was incubated with 15 μg of dsRNA. After a 1-h incubation at 24 °C, 2 ml of medium supplemented with 15% FBS was added to each culture. Control cultures were prepared in the same way but without addition of dsRNA. Both RNA-treated and control cells were processed for total RNA isolation, protein extraction, and cytological analysis. The RNAi experiments were repeated three times to confirm the reproducibility of the observations.

qRT-PCR analysis

Total RNA purified according to the protocol supplied with Qiazol Reagent (Qiagen) was reverse transcribed using oligo dT and SuperScript reverse transcriptase III (Invitrogen).

The qPCR reactions were carried out with QuantiFast SYBR Green PCR Kit (Qiagen) according to manufacturer's protocol. For the quantification of *ash1*, *nej*, and *trx* transcripts, we used the $2^{-\Delta\Delta Ct}$ method by comparing their amount to *Rpl32* transcript. qRT-PCR experiments were performed in three independent biological replicates each with three technical replicates. Statistical significance was determined by unpaired two-tailed Student's *t* test. A *p* value < 0.05 was considered statistically significant.

The primers used were:

> *ash1* F 5′-ACACCATTTCCTGCGTCCT-3′
> *ash1* R 5′-TGAGAAGAACCTTGCCGTCT-3′
> *nej* F 5′-GCGTCATTTGCTATCCCTTC-3′
> *nej* R 5′-CTTGCTTGCCATCCACTACC-3′
> *trx* F 5′-CAGGGACGCAAAACTAAGGA-3′
> *trx* R 5′-TGATAGGGCTCACAACAGCA-3′
> *Rpl32* F 5′-GCGCACCAAGCACTTCATC-3′
> *Rpl32* R 5′-TTGGGCTTGCGCCATT-3′

Western blot

Cells were homogenized in SDS gel-loading buffer (60 mM Tris-HCl, pH 6.8, 10% glycerol, 2% SDS, 10 mM dithiothreitol, and 0.1% bromophenol blue) in the presence of protease inhibitors (10 μM benzamidine HCl, 1 mM PMSF, 1 μg/ml phenanthroline, 10 μg/ml aprotinin, 10 μg/ml leupeptin, and 10 μg/ml pepstatin A) and heated at 95 °C for 5 min. Lysates were analyzed by 10% SDS-PAGE and transferred onto Immobilion-P polyvinyldifluoride membranes (Bio-Rad Laboratories) in CAPS-based transfer buffer (10 mM CAPS, pH 11, and 10% methanol) in a semi-dry transfer apparatus (Amersham Biosciences). The filter was blocked with 5% non-fat dry milk in Tris-buffered saline with Tween 20 (TBST) buffer (20 mM Tris, pH 7.5, 150 mM NaCl, and 0.1% Tween 20) and incubated with antibodies against Cid (1:500, Active Motif #39713) and α-tubulin (1:4000, Sigma #T5168). The membranes were subsequently incubated with a 1:10000 dilution of horseradish peroxidase–conjugated anti-mouse or anti-rabbit antibodies. The enhanced chemiluminescence kit was purchased from GE Healthcare. Images were acquired with the ChemiDoc system (Bio-Rad Laboratories).

Chromosome preparations from cultured cell lines and larval neuroblasts

Mitotic chromosomes from S2 and ML-DmBG2-C6 cells were prepared by an air-drying method. Briefly, after phosphate-buffered saline (PBS) washing and centrifugation, hypotonic solution (sodium citrate 0.5%) was added gently to the wall of the tube, and cells were incubated for 10 min at room temperature. The cells were then centrifuged again and supernatant was removed; cells were then fixed for 7 min by adding 3:1 (*v:v*) ice-cold mix of methanol and acetic acid dropwise. After removing the supernatant, the cellular pellet was resuspended in 200 μl of fixative solution and 10 μl was spread on a microscope slide and air-dried.

For indirect immunofluorescence experiments, S2 cells were incubated in 10^{-5} M colchicine for 2 h, centrifuged to remove the supernatant, washed in 1X PBS, and fixed for 7 min in 1X PBS and 3.7% formaldehyde. In this case, mitotic chromosomes were prepared by centrifuging cells onto the slides at 900 rpm for 4 min using a Cytospin™ 4 centrifuge (Thermo Fisher Scientific). The slides were then frozen in liquid nitrogen, washed in 1X PBS for 5 min, permeabilized in 1X PBS and 1% Triton-X100 for 10 min, blocked in 1X PBS and 5% non-fat dried milk for 30 min, and processed for immunofluorescence with rabbit anti-Cid (1:500, Active Motif #39719) or mouse anti-α-tubulin (1:100, Sigma) antibodies as described below.

Mitotic chromosomes from brains were prepared according to Fanti and Pimpinelli (2004). Briefly, brains were dissected from third instar larvae in physiological solution (NaCl 0.7%) and transferred to hypotonic solution (sodium citrate 0.5%) for 8 min. Brains were then transferred to a drop of chromosome isolation buffer (6 mM $MgCl_2$, 1% citric acid, and 1% Triton-X100), placed on a siliconized coverslip, dissociated using syringe needles, and squashed in the same solution. Slides were frozen in liquid nitrogen, transferred to cold methanol at − 20 °C for 5 min and then in acetone at − 20 °C for 1 min, washed in 1X PBS for 5 min, permeabilized in 1X PBS and 1% Triton-X100 for 10 min, blocked in 1X PBS and 5% non-fat dried milk for 30 min, and processed for immunofluorescence with rabbit anti-Cid (1:500, Active Motif).

Interphase nuclei preparations

Nuclei were prepared by centrifuging 1.2×10^5 cells/ml onto slides at 800 rpm for 4 min using a Cytospin™ 4 centrifuge; the slides were fixed in 4% paraformaldehyde for 10 min, washed in 1X PBS for 5 min, and blocked in 1X PBS, 1% BSA, and 0.5% Triton-X100 for 30 min before incubation with appropriate primary antibodies.

Chromatin fiber preparations

Chromatin fibers from S2 cells were prepared, and slides were processed for immunofluorescence as described in Blower et al. (2002). In brief, chromatin fibers from S2 cells were prepared by centrifuging 1.2×10^5 cells/ml onto slides at 800 rpm for 4 min using a Cytospin™ 4 centrifuge (Thermo Fisher Scientific); the slides were then dipped in salt lysis buffer (25 mM Tris at pH 7.5, 500 mM NaCl, and 1% Triton-X100) for 10 min and fixed in 4% paraformaldehyde for 10 min. Slides were washed in 1X PBS for 5 min and blocked in 1X PBS, 1% BSA, and 0.5% Triton-X100 for 30 min before incubation with appropriate primary antibodies.

Immunofluorescence assays

Incubation with the primary antibody was carried at room temperature for 1 h and at 4 °C overnight. The primary antibodies were diluted in 1X PBS and 1% BSA as follows: rabbit anti-Ash1 (1:40, Tripoulas et al. 1996), rabbit anti-Trx (1:50, Rozenblatt-Rosen et al. 1998; Petruk et al. 2001), rabbit anti-CBP (1:100, Petruk et al. 2001), mouse anti-histone H3K27ac (1:300, Active Motif #39685), mouse anti-histone H3K4me2 (1:100, Active motif #39679), mouse anti-H3K27me3 (1:200, Active Motif #61017), rabbit anti-Cid (1:500, Active Motif), chicken anti-Cid (1:100, Blower and Karpen 2001), rat anti-H3 (1:70 Active Motif #61648), and mouse anti-tubulin (1:100, Sigma).

For double immunostaining experiments, we used the following combinations: (1) rabbit anti-Ash1, rabbit anti-CBP, and rabbit anti-Trx were used in combination with chicken anti-Cid; primary antibodies were detected with Alexa Fluor 488 goat anti-rabbit (1:300) and Alexa Fluor 555 goat anti-chicken (1:300) (both from Thermo Fisher Scientific); (2) mouse anti-H3K27ac, anti-H3K4me2, and anti-H3K27me3 were used in combination with rabbit anti-Cid, and detection was carried out with Cy^3-linked goat anti-mouse (1:400, Jackson ImmunoResearch) and Alexa Fluor 488 goat anti-rabbit (1:300, Thermo Fisher Scientific); (3) rat anti-H3 was used in combination with rabbit anti-Cid, and detection was carried out with Cy^3-linked goat anti-rat (1:400, Jackson ImmunoResearch) and Alexa Fluor 488 goat anti-rabbit (1:300). Primary anti-tubulin antibodies were detected with Cy^2-linked goat anti-mouse (1:50, GE Healthcare). The incubation with secondary antibodies was carried out at room temperature for 2 h. Washes during immunostaining were 3 × 5 min in 1X PBS. After immunostaining preparations were counterstained with 0.1 µg/ml of 4^1,6-diamidino-2-phenylindole (DAPI), dissolved in 2XSSC for 5 min for mitotic chromosomes and 30 min for chromatin fibers, and mounted in Vectashield (Vector Laboratories).

Chromosomes and fiber preparations were captured at the same exposure time using a computer-controlled Zeiss microscope equipped with a cooled CoolSnap CCD camera. The fluorescent signals, recorded separately as gray scale digital images, were pseudocolored and merged using Adobe Photoshop.

The fluorescence quantification of Cid at the kinetochore/nucleus was performed using ImageJ Software. To estimate the fluorescence intensity of the Cid antibody signal, we established a circular region with fixed dimensions that included the Cid spots. For each cell, we measured at least four Cid signals in the centromere/nuclei region and one outside of the cell (background signal) in proximity of the region chosen for the analysis. A background subtraction was performed for each intensity area of Cid measured.

The number of the fluorescent spots on the fibers was counted with two different methods. With the first method, about 150 fibers were analyzed and the spots were counted using ImageJ Software (Automatic Particle Analysis). Then, a more accurate analysis on a reduced number of fibers was done using a manual method. The spots of an approximate length of 0.25 μm were counted on enlarged images. For spots longer than 0.25 μm, the signals were counted using Photoshop Software (ruler tool) to measure the spot length and dividing by 0.25 μm. With both methods, the values of statistical significance remained unchanged.

Generation of S2 cells stably expressing SNAP-tagged Cid

S2 cells were co-transfected with pSNAP-Cid (gift of A. Lusser) and pCoHygro (gift of P. Somma) using Effectene™ Transfection Reagent (Qiagen) following the manufacturer's instructions. A stable cell line expressing SNAP-Cid was generated by selection with 500 μg/ml hygromycin B (Sigma).

Quench-chase-pulse labeling of newly synthesized Cid in *nej* and *Ash1* RNAi-depleted cells

S2 cells stably expressing SNAP-tagged Cid were diluted at 1×10^6 cells/ml and transfected with dsRNA against *nej* or *ash1* using Cellfectin II reagent (Invitrogen) following the manufacturer's instructions. Seventy-two hours after transfection, growth medium was removed and RNAi cells (and mock-transfected control cells) were incubated with 0.9 μM SNAP-Cell Block (NEB) in fresh S2 medium for 30 min at 25 °C. Cells were then washed three times (5 min each) in fresh medium before addition of S2 medium supplemented with 10 μM $CuSO_4$ to induce production of SNAP-Cid. After a 24-h chase period, the medium was removed and pulse labeling of newly synthesized SNAP-Cid was performed by incubation with 4.5 μM SNAP-Cell TMR Star (NEB) in fresh medium for 30 min. Non-reacted TMR Star was removed by washing cells 3 times for 5 min each with fresh medium before fixation in 5% paraformaldehyde/0.3% Triton-X100 in 1X PBS. Fixed cells were resuspended in 1X PBS and deposited onto a clean slide using a Cytospin™ 4 centrifuge (Thermo Fisher Scientific) at 900 rpm for 4 min. All slides were counterstained with DAPI (4,6-diamidino-2-phenilindole, 0.01 mg/ml) and mounted in anti-fading medium (23.3 mg/ml of DABCO (Sigma Aldrich) in 90% glycerol/1% PBS).

Statistical analyses

Fisher's exact test, one-way ANOVA test, and Dunnett's multiple comparisons test were used to determine statistical significance. p values < 0.05 were considered statistically significant. Statistical analyses were performed using GraphPad Prism version 6.00 for Windows (GraphPad Software, La Jolla, CA, USA, www.graphpad.com).

Results

Proteins of the Trx-G complex are required for chromosome condensation and segregation

We have previously shown that proteins of the Trx-G and Pc-G complexes localize to the heterochromatic regions and the
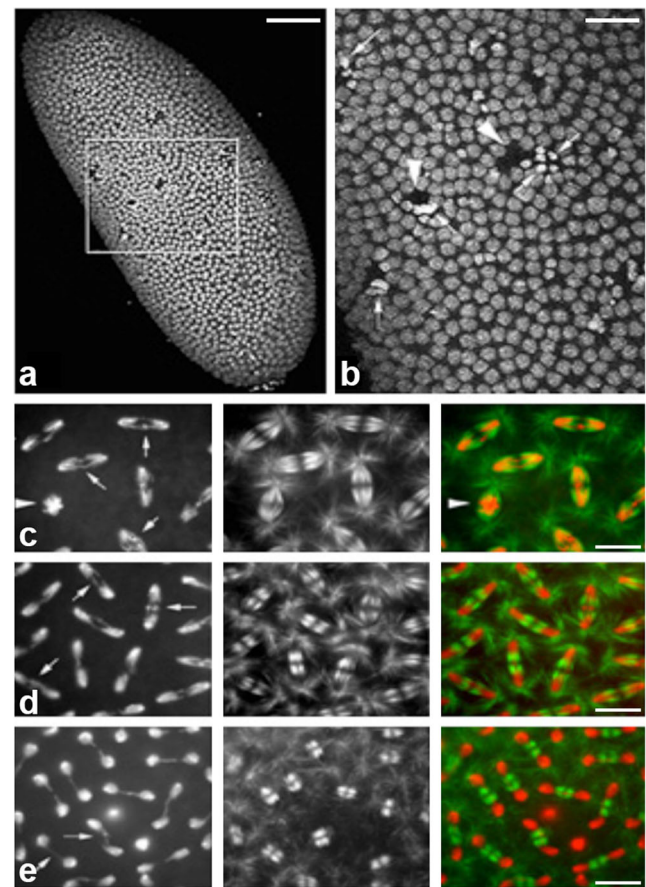
Fig. 1 Confocal images of an embryo derived from crosses between *ash1/+* parents showing abnormalities in chromosome condensation and segregation. **a** Whole embryo with blastoderm regions devoid of cells suggesting migration of damaged nuclei towards the interior of the embryo (scale bar indicates 150 μm). **b** Enlarged image showing "holes" (arrowheads) in the blastoderm and overcondensed nuclei that will probably fall down into the embryo interior (arrows) (scale bar indicates 50 μm). **c–e** Early anaphases (**c**), late anaphase (**d**), and telophase (**e**) stained with propidium iodide (left) and with antibodies against tubulin (middle). In the merged images on the right, DNA (propidium iodide) is red and tubulin green. The arrowhead in (**c**) indicates collapsed chromosomes; the arrows in (**c–e**) indicate chromosome bridges and lagging chromosomes (scale bars indicate 10 μm)
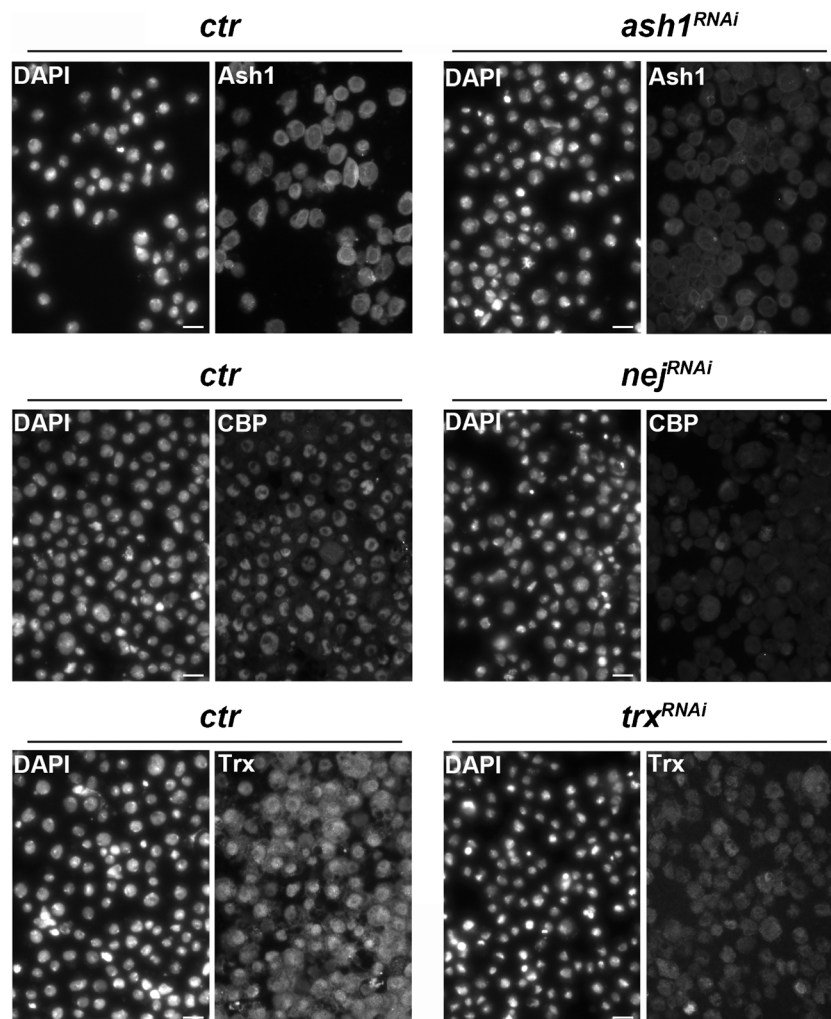
Fig. 2 Immunostaining of Ash1, CBP, and Trx in nuclei from S2 cells in which *ash1*, *trx*, or *nej* were silenced by RNA interference. For each panel from left to right: DAPI staining and Trx-G protein pattern in control cells, DAPI staining, and Trx-G protein pattern in the RNAi cells; from top to bottom: Ash1, CBP, and Trx. Scale bars indicate 20 μm

centromeres (Fanti et al. 2008). These findings prompted us to ask whether these proteins have roles in chromosome organization and centromere function. We focused on the Trx-G proteins Ash1 and Trithorax (Trx) and the Pc-G protein Polycomb (Pc) and analyzed the effects of null mutations in their coding genes. Since these mutations cause early lethality, we examined the phenotypes of the embryo progeny from inter se crosses ($n = 200$ per cross) between $ash1^{06}$/+, trx^{B16}/+, and Pc^{1}/+ heterozygotes. We found substantial alterations in chromosome condensation and anaphase chromatin bridges in approximately 20% of the embryos from $ash1^{06}$/+ (Fig. 1) and trx^{B16}/+ parents (data not shown), while embryos from Pc^{1}/+ parents were not distinguishable from wild-type embryos (data not shown). The finding that the observed frequencies of embryos with chromosome abnormalities are close to the expected frequency of homozygous mutant embryos strongly suggests homozygosity for either *ash1* or *trx* results in chromosome instability, and their maternally supplied products are not sufficient to ensure normal chromosome behavior. Similar results have been shown also in embryos from *ph*/+ (Lupo et al. 2001) and *Trl*/+ (Bhat et al. 1996) heterozygous parents.

To further explore the mitotic roles of the proteins of the Trx-G complex, we silenced by RNA interference (RNAi), *ash1*, *trx*, and *nej* (encoding CBP) in the S2 (Fig. 2) and ML-DmBG2-C6 tissue culture cells (data not shown) derived from late embryonic stages (Schneider 1972) and from the larval central nervous system (Ui et al. 1994), respectively. In both cell lines, *ash1*, *trx*, or *nej* silencing caused very high frequencies of metaphases with an abnormal chromosome condensation and anaphases and telophases with lagging chromosomes and multiple chromatin bridges (Fig. 3a, b, Supplementary Fig. 1). In addition, in cells depleted of Ash1, Trx, or CBP, the ratio of metaphase/prometaphase figures was significantly lower than in the control (Fig. 3c) suggesting

Fig. 3 RNAi-mediated silencing of *ash1*, *nej*, and *trx* affects chromosome condensation and segregation in S2 cells. **a** Metaphases (left), anaphases (the two central images), and telophases (right). Note the abnormal condensation of metaphase chromosomes and the bridges and lagging chromosomes in anaphases and telophases. Scale bars indicate 10 μm. **b** Frequencies of metaphases with abnormally condensed chromosomes (*ctr* n = 204, *ash1* n = 258, nej n = 280, *trx* n = 233) and of ana-telophases with bridges and lagging chromosomes (ctr n = 98, *ash1* n = 170, nej n = 139, *trx* n = 148). **c** Metaphase/prometaphase ratios (ctr n = 641, *ash1* n = 850, nej n = 451, *trx* n = 718). Statistical significance was determined using Fisher's exact test ($p < 0.0001$)
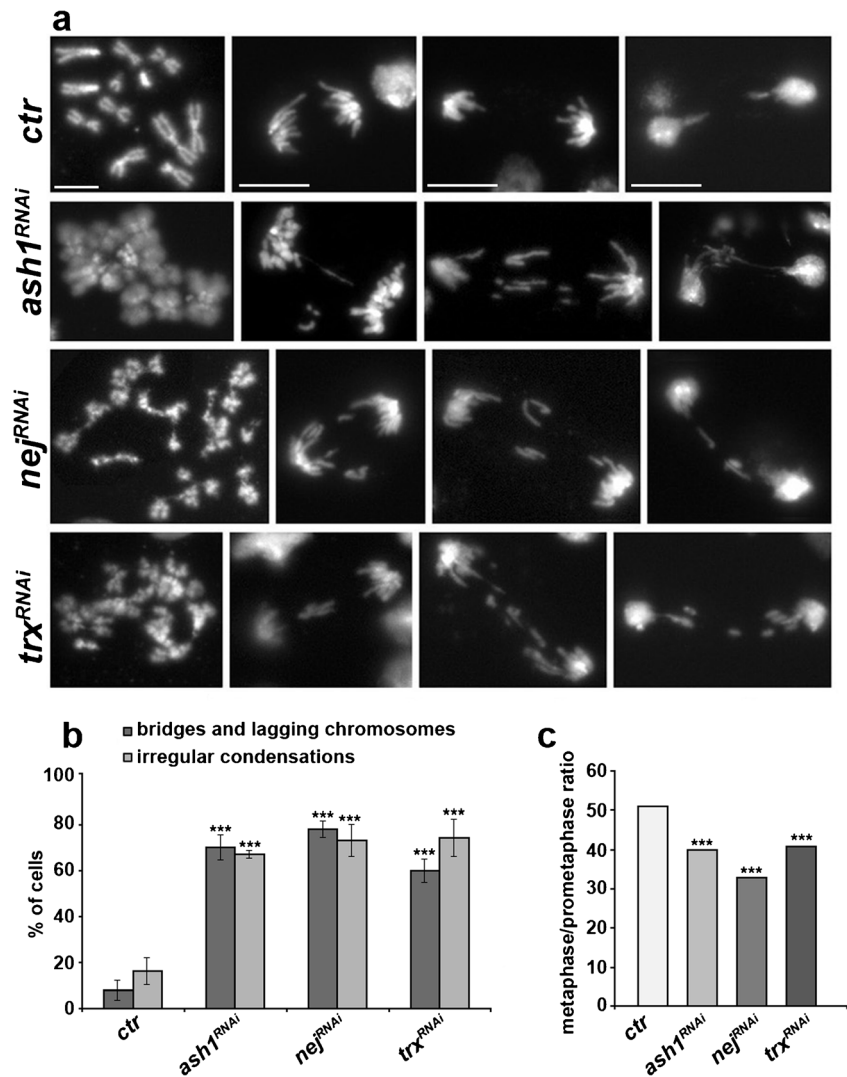
a longer permanence in prometaphase or a defect in chromosome alignment at metaphase (Somma et al. 2008). We also observed a low but statistically significant increase in cells showing premature sister chromatid separation (9% in *nej* and 4% in both *ash-1* and *trx* RNAi cells) compared with controls, in which this phenotypic trait was virtually absent (Supplementary Fig. 2). This phenotype could be an indication of an abnormal centromeric function, since Cid is required for the recruitment of the Mei-S332 protein that maintains sister chromatid cohesion at centromeres (Blower and Karpen 2001; reviewed in Meluh and Strunnikov 2002). The defects in chromosome segregation are also evident in mitotic cell immunostained for tubulin to visualize the spindle. The spindles of these cells do not show gross morphological defects due to microtubule organization suggesting that RNAi-mediated depletion of Ash1, Trx, or CBP does not affect spindle assembly (Fig. 4).

Together, these results show that cells depleted for Ash1, Trx, and CBP are defective in chromosome alignment and segregation, suggesting an underlying defect in centromere or kinetochore structure.

The Trx-G centromeric proteins have a role in Cid loading

The phenotypes observed in cells depleted of components of the Trx-G complex and the localization of these proteins in the centromeric regions (Fanti et al. 2008) prompted us to ask whether the Trx-G proteins are required for Cid localization at centromeres. To address this question, we first examined suitably immunostained extended chromatin fibers from S2 control cells to visualize the localization of Trx, Ash1, and CBP in the centromeric regions marked by Cid (Fig. 5). We define as centromeric region in the fiber (CRF) a fiber segment containing multiple Cid signals flanked by regions not

Fig. 4 Silencing of *trx*, *ash1*, and *nej* does not affect the assembly of the mitotic spindle in S2 cells. From left to right, each panel shows DAPI staining, tubulin staining, and merged images; from top to bottom, metaphases, anaphases, and telophases. In *trx*, *ash1*, and *nej* RNAi cells, spindle microtubules are well organized and spindle deformations are due to defects in chromosome segregation. Scale bars indicate 10 μm
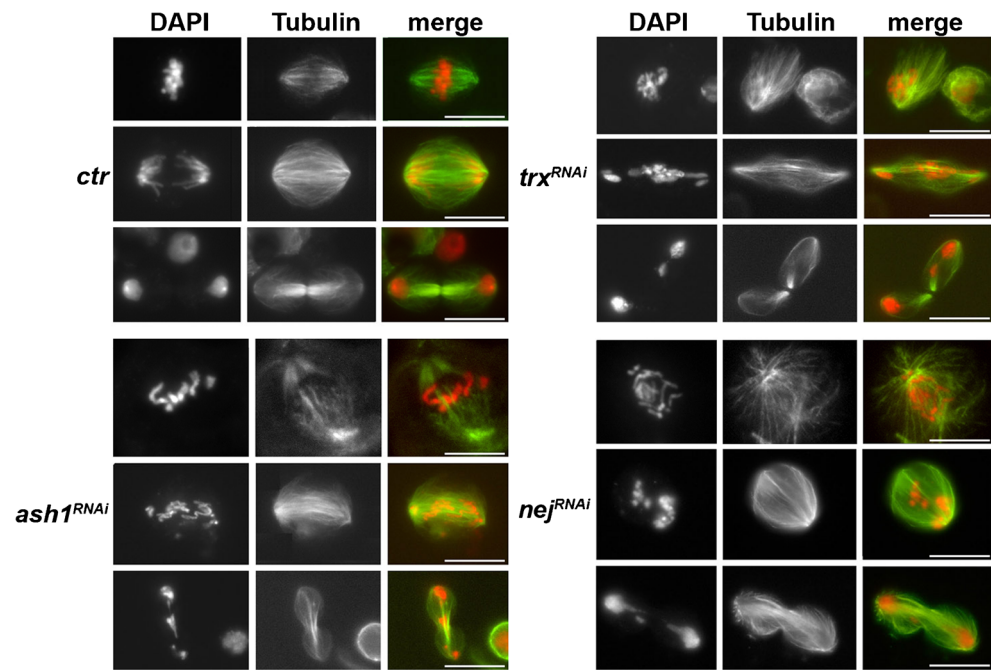
containing Cid signals and having at least one-third the length of the CRF. Trx, Ash1, and CBP localized in CRFs; CBP and to lesser extent Trx and Ash1 also co-localized with Cid in about 22% and 28%, respectively, of sites along the CRF (35% for CBP). However, most CBP, Trx, and Ash1 immunosignals were located in sites adjacent to Cid signals (Fig. 5). Furthermore, we examined also their localization in interphase S2 cells ($n = 150$) (Supplementary Fig. 3). In both cases, we observed that virtually all the Cid-containing regions are also immunostained with the Trx-G proteins. These results suggest a functional relation between Cid and the Trx-G proteins in centromeric regions.

We next tested whether Cid and the proteins of the Trx-G complex are functionally related. We immunostained for Cid mitotic chromosomes from the larval brain of $ash1^6/ash1^{22}$ mutants and from the brains of larvae bearing a *nej* RNAi construct driven by a heat shock–inducible *Gal4* driver (Smolik and Jones 2007) and a trx RNAi construct driven by elav-Gal4 (Fig. 6). We observed a decrease of the Cid protein at the centromeres of all chromosomes in both Ash1- and CBP-deficient brains. A similar result was obtained by examining larval brain chromosomes from $ash1^6/+$ heterozygous larvae also carrying *nej* silenced by the heat shock–inducible *Gal4* driver. Unlike in Ash1- and CBP-deficient brains, the amount of Cid increases at the centromere of the chromosomes in Trx-deficient brains (Fig. 6a, b). It was not possible to extend the analysis to brains from *trx* and *nej* mutants because homozygotes for null alleles in these genes die before reaching the third instar larval stage.

To confirm and extend the results obtained with larval brains, we performed RNAi in S2 cells against each of the 3

genes (*ash1*, *trx*, and *nej*) followed by Cid immunostaining (Fig. 7 and Supplementary Fig. 4). Quantification of the Cid fluorescence intensity (in at least 100 mitotic figures per sample) showed that Ash1- and CBP-depleted chromosomes exhibit a significant decrease in Cid fluorescence at centromeres compared with controls. In contrast, Trx-depleted cells did not show a significant reduction in Cid staining. Double RNAi against *nej* and either *ash1* or *trx* resulted in decreased Cid fluorescence compared with controls. Double RNAi against *ash1* and *trx* unexpectedly caused a strong increase in Cid fluorescence at mitotic centromeres (Fig. 7a, b). This result was confirmed also when the fluorescence intensity of Cid was examined in the interphase nuclei, suggesting that this difference is not related with the cell cycle (Fig. 7a, c). Importantly, these abnormalities in Cid localization at centromeres do not depend on a reduced intracellular quantity of the Cid protein, because western blotting analysis showed that *ash1*, *nej*, and *trx* RNAi cells (Fig. 7d for a control of RNAi efficiency) and untreated cells exhibit Cid levels that are not significantly different (Fig. 7e, f).

To obtain further insight into the role of Trx-G proteins in Cid deposition, we extended our analysis to chromatin fibers of S2 cells (Fig. 8). For both control and RNAi cells, we counted the number of discrete Cid spots in CRFs with a wide range of lengths and long enough to check that they were on a single chromatin fiber (Fig. 8a). We define a spot as a fluorescent signal about 0.25 μm long. The number of spots was counted taking into account the signal lengths but not the intensity of fluorescence. In control CRFs, we found an average of 36.66 spots; the average numbers of these spots were significantly decreased in CRFs from *ash1* (24.81) and *nej*
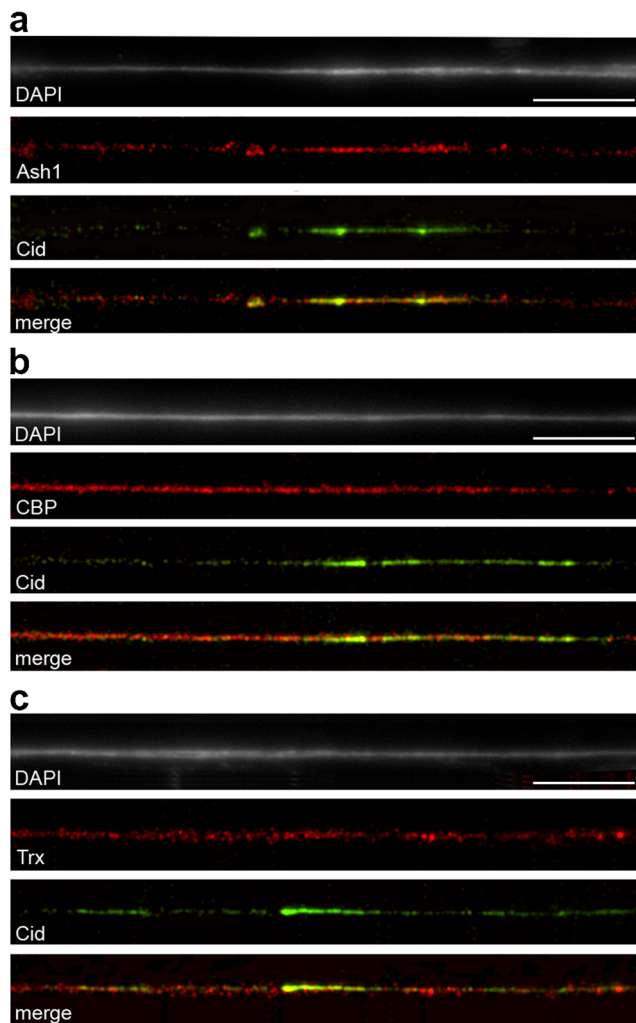
Fig. 5 Localization of Ash1, CBP, and Trx in stretched chromatin fibers enriched in Cid. For each panel, from top to bottom: DAPI staining, Trx-G protein in red, Cid in green, and merged image of Cid with respectively **a** Ash1 (*n* fibers = 83), **b** CBP (*n* = 78), and **c** Trx (*n* = 85). Note that Ash1, CBP, and Trx localize in the centromeric regions marked by Cid, but most of their signals are located in sites adjacent to Cid signals. Scale bars indicate 10 μm

(25.26) RNAi cells, as well as in CRFs from *ash1 nej* (21.19) double RNAi cells. The numbers of Cid spots found in CRFs from *trx* RNAi cells (35.52) and in both *nej trx* (30.73) and *ash1 trx* (32.49) double RNAi cells were not significantly different from controls (Fig. 8b). We also measured the average lengths of CRFs and the average densities of Cid spots in CRFs (spots number/CRF length). Importantly, the lengths of the CRFs showed comparable normal distributions in all cases (39.60 μm for the control; 39.08 μm for *ash1*; 35.80 μm for *nej*; 35.79 μm for *trx*; 36 μm for *ash1 trx*; 37.31 μm for *nej trx*) except in *ash1 nej* double RNAi cells where CRFs were significantly shorter (24.68 μm) (Fig. 8c–e). Thus, the CRF analysis is in good agreement with the measures of Cid fluorescence intensity performed on mitotic chromosomes but did

not confirm the increase in Cid fluorescence observed in *ash1 trx* double RNAi cells.

In order to understand whether Ash1 and CBP have a role in Cid maintenance or in its deposition at the centromere, we silenced by RNA interference, *ash1*, and *nej* in S2 cells and performed a quench-chase-pulse labeling of newly synthesized Cid using a Snap-Cid plasmid (Boltengagen et al. 2016). We analyzed about 100 nuclei and observed a significant decrease in TMR-Cid fluorescence intensity in cells depleted for Ash1 and CBP with respect to the control (Fig. 9). Taken together, these results show that Ash1 and CBP proteins have a role in Cid loading.

The Trx-G proteins modify histone tails in centromeric regions

The Trx-G and Pc-G complexes regulate gene expression by post-translational modifications of the histone tails. Trx and Ash1 have both a methyltransferase activity while CBP has a specific acetyltransferase activity on H3K27 (Tie et al. 2009). Based on these results, and on the finding that mammalian p300/CBP is present at centromeres (Craig et al. 2003), we investigated whether CBP acetylates centromeric histones and the relationship between this epigenetic modification and Cid loading. To address this issue, we analyzed the immunopatterns in CRFs doubly immunostained for H3K27ac and Cid in S2 cells (Fig. 10a). In control cells, we observed prominent H3K27ac signals localized in the CRF and in the CRF flanking regions. The H3K27ac signals were mostly not coincident with Cid signals, as the H3 nucleosomes are interspersed with Cid nucleosomes. For both control and *ash1*, *nej*, and *trx* RNAi cells, we counted the number of discrete H3K27ac spots and we also measured the average length of CRFs and calculated the average densities of H3K27ac spots. In control CRFs, we found an average of 10.12 spots in 10 μm. In CBP-depleted cells, we observed a substantial decrease in the H3K27ac signals with respect to control cells (an average of 3.91 spots in 10 μm) (Fig. 10b). This result is particularly interesting, as previous work has shown that the H3K12ac is virtually absent at the CRFs (Sullivan and Karpen 2004). As expected, in *ash1* and *trx* RNAi cells, the centromeric H3K27ac localization in CRFs was similar to that in control cells (an average of 9.10 and 10.37 spots in 10 μm, respectively).

In order to verify if H3K27ac was replaced by H3K27me, we analyzed the immunopatterns of H3K27me3 and Cid in CRFs from S2 cells depleted for CBP. In *nej* RNAi cells, the centromeric H3K27me3 localization in CRFs was similar to that in control cells (Supplementary Fig. 5).

We also analyzed the immunopatterns in CRFs doubly immunostained for H3K4me2 and Cid (Fig. 10c). In control CRFs, we found an average of 7.08 spots in 10 μm. In Ash1-depleted cells, we observed a decrease in the
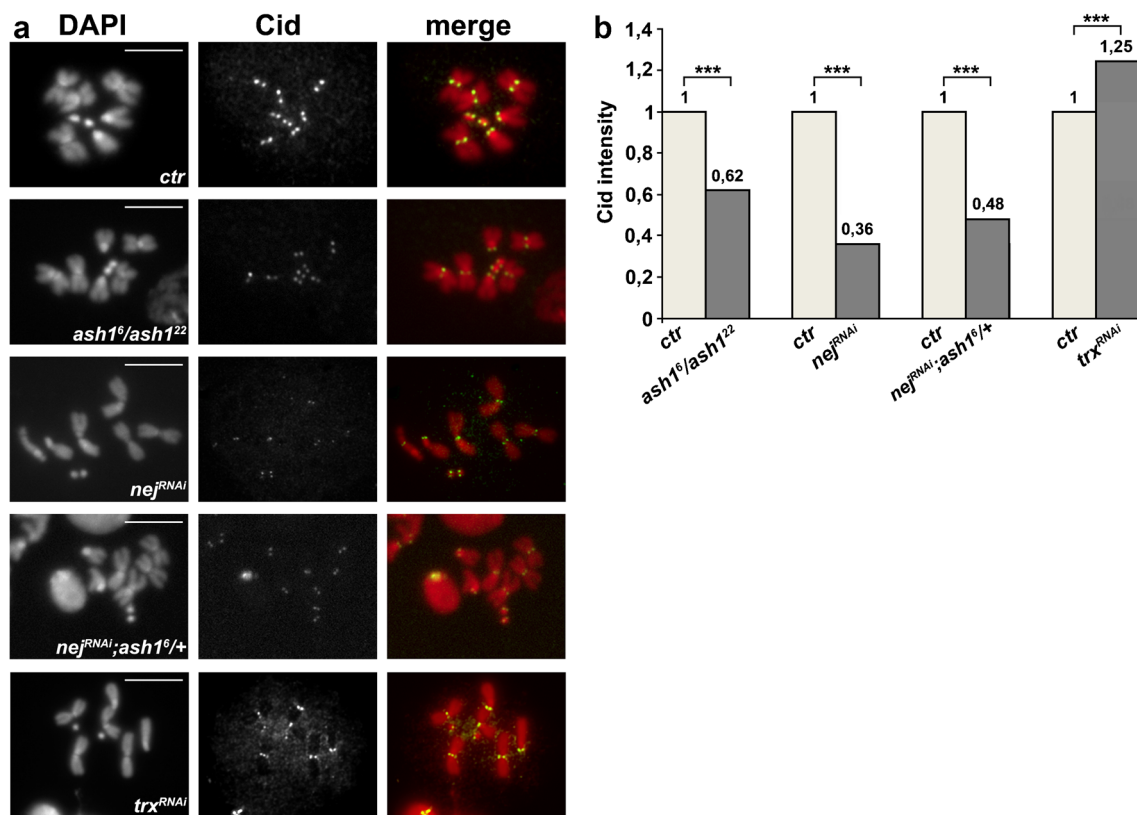
Fig. 6 Ash1 and CBP depletion leads to a decrease in the amount of Cid associated with centromeres, while Trx leads to Cid increase. **a** Examples of mitotic chromosomes immunostained for Cid from control ($n = 553$), $ash1^6/ash1^{22}$ ($n = 181$), nej^{RNAi} (UAS-nej^{RNAi}; hs-$Gal4/+$) ($n = 171$), nej^{RNAi}; $ash1^6/+$ (UAS-nej^{RNAi}; hs-$Gal4/+$; $ash1^6/+$) ($n = 535$), and trx^{RNAi} ($elav$-$Gal4/+$; $UAS\ trx^{RNAi}$ /+) ($n = 253$) brains. In merged images, Cid is green and DNA red. Note the strong decline in the fluorescence intensity of Cid signals in all three mutant conditions of $ash1$ and nej. Scale bars indicate 10 μm. **b** Quantification of the amount of Cid associated with the mitotic chromosomes from Ash1, CBP, and Trx-depleted brains; statistical significance was determined using Fisher's exact test (***$p < 0.001$)

H3K4me2 signals compared with control cells (3.25 spots in 10 μm), while in the CRFs from CBP- and Trx-depleted cells, the H3K4me2 signals were not significantly different to those of control cells (an average of 6.13 and 6.53 spots in 10 μm) (Fig. 10d).

In order to verify that the patterns of H3K27ac and H3K4me2 are specifically involved in Cid deposition and their reduction is not a generic consequence of Cid dysfunction, we also analyzed the immunopatterns in CRFs doubly immunostained for Cid and H3K27ac or H3K4me2 in Cid-depleted S2 cells. In both cases, we did not observe any significant difference compared with the control (Supplementary Fig. 6).

Finally, to ascertain if the observed decrease of H3K27ac and H3K4me2 in respectively CBP- and Ash1-depleted cells is due to a general loss in histones at the centromeres, we analyzed the immunopatterns in CRFs doubly immunostained for H3 and Cid in the S2 cells (Fig. 11a). For both control and RNAi cells, we counted the number of discrete H3 and Cid spots and calculated the ratio between the average number of Cid and H3 spots. Cid/H3 ratio was significantly lower for all the Trx-G proteins compared with the control (Fig. 11b).

Moreover, in Ash1- and CBP-depleted cells, the average number of H3 spots was similar to that observed in control cells. As expected, the average number of Cid spots was significantly lower compared with the control.

Conversely, in Trx-depleted cells, the average number of H3 was significantly higher than that in controls. No difference we observed in the average number of Cid spots compared with the control. This result in Trx-depleted cells could explain the presence of segregation defects without a concomitant impairment of Cid deposition.

Discussion

### Trx, Ash1, and CBP are new components of Cid loading machinery

Although several proteins involved in the proper CENP-A deposition have been identified in various organisms, the complete network of molecular determinants and epigenetic marks involved in this process remains to be defined. For example, studies in fission yeast have shown Mis18 as an
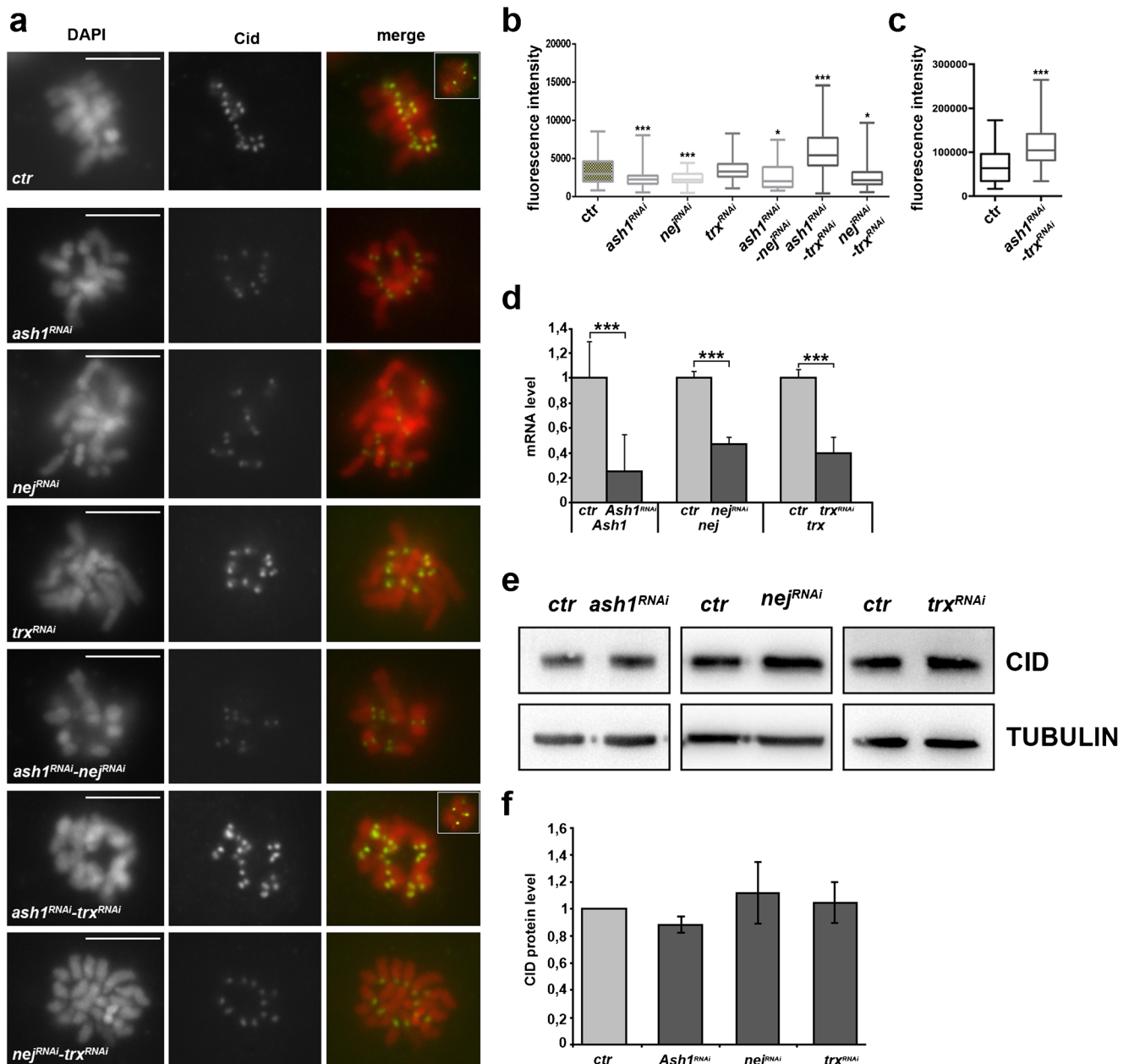
Fig. 7 RNAi against the Trx-G protein coding genes affects Cid recruitment at centromeres of S2 cell chromosomes. **a** From left to right: DAPI staining, anti-Cid immunostaining, and merged images; from the top to bottom: control metaphase and *ash1*, *nej*, *trx*, *ash1-nej*, *ash1-trx*, and *nej-trx* silenced metaphases. Note the different fluorescence intensity among the different interfering cells. In particular, the fluorescence intensity decreases in *ash1*, *nej*, *ash1-nej*, and *nej-trx* interfered cells, with respect to the control; it is similar in *trx*^{RNAi} cells and increases in *ash1*^{RNAi}-*trx*^{RNAi} cells, with respect to the control. Scale bars indicate 10 μm. In the window of the *ctr* and *ash1*^{RNAi}-*trx*^{RNAi} fluorescence pattern of Cid in a nucleus. **b** Graphic representation of Cid fluorescent spots in S2-interfered metaphases for above gene combinations ($n = 120$ for *ctr*, *ash1*, *ash1-nej*, and *ash1-trx*; $n = 98$ for *nej*; $n = 124$ for *trx*; $n = 108$ for *nej-trx*). Statistical significance was determined by ANOVA test ($F =$ 59.35; ***$p < 0.001$) and Dunnett's multiple comparisons test (*$p < 0.05$; ***$p < 0.001$). **c** Graphic representation of Cid fluorescent spots in the control and *ash1*^{RNAi}-*trx*^{RNAi} interphase nuclei. Statistical significance was determined using unpaired two-tailed Student's *t* test (***$p < 0.001$). **d** qRT-PCR analysis showing the significant decrease in *ash1*, *cbp*, and *trx* RNAs. Fold changes in RNA levels relative to control were normalized to Rpl32 levels. Error bars indicate SEM from three biological replicates (unpaired two-tailed Student's *t* test ***$p < 0.001$). **e** Western blot analysis of Cid protein in *ash1*, *cbp*, and *trx* RNAi S2 cells. **f** The densitometry analysis was performed on three biological replicates and showed no significant difference in Cid protein with respect to the control. One-sample *t* test was employed as the statistical method on three biological replicates. $p < 0.05$ was considered to be statistically significant ($p = 0.27$ for *ash1*^{RNAi}; $p = 0.69$ for *nej*^{RNAi}; $p = 0.46$ for *trx*^{RNAi})
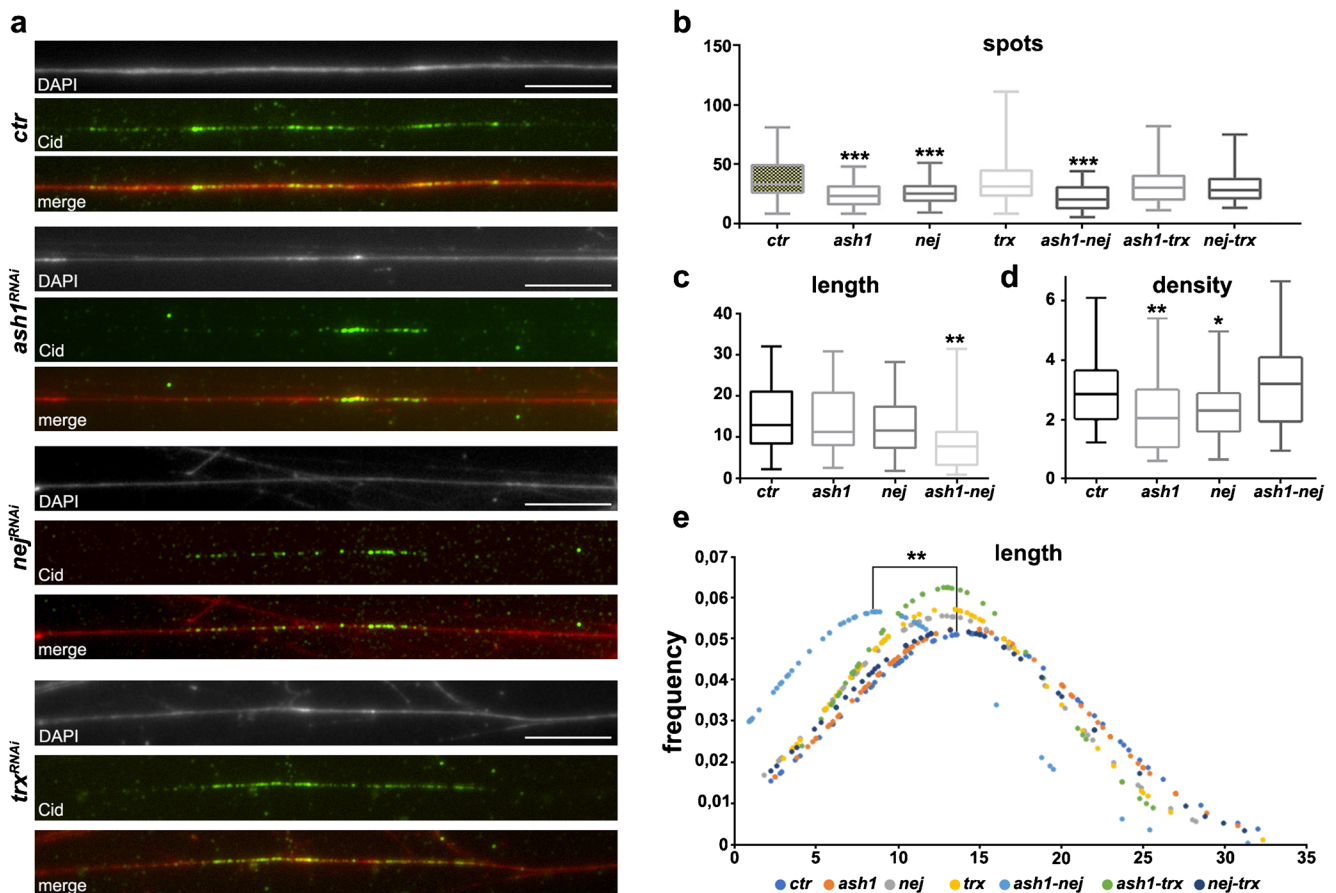
Fig. 8 Ash1 and CPB depletion leads to a decrease in the amount of Cid associated with centromeres also in extended fibers. **a** Immunostaining of extended chromatin fibers from S2 cells with anti-Cid antibodies. From the top to bottom, for the control and for each silenced gene (in the order *ash1*, *nej*, and *trx*), an extended fiber DAPI stained, Cid immunosignals pseudocolored in green, and merged images in which the DNA fiber is pseudocolored in red are shown. Note the strong decrease of Cid immunosignals in *ash1*- and *nej*-silenced fibers with respect to the control and the *trx*-silenced fiber. Scale bar indicates 10 μm. **b** Graphic representation of the number of Cid fluorescent spots in S2 cells in which above genes combination are silenced. **c** Graphic representation of difference in

centromere length for the control, *ash1*, *nej*, and *ash1-nej*. For all the other not shown combinations, differences are not significant. **d** Graphic representation of difference in density of the Cid spots. For all the other not shown combinations, differences are not significant. **e** Normal distribution function of length values for each genotype. Statistical significance was determined by ANOVA test on *n* of analyzed fibers = 53 for *ctr*, 69 for *ash1*, 48 for *nej*, 52 for *trx*, 44 for *ash1 nej*, 41 for *ash1 trx*, and 44 for *nej trx* ($F = 8.914$, ***$p < 0.001$ for spots; $F = 2.814$, *$p < 0.05$ for length; $F = 4.834$, ***$p < 0.001$ for density) and Dunnett's multiple comparisons test (***$p < 0.001$; **$p < 0.01$; *$p \leq 0.05$)

important factor for CENP-A loading at centromeres (Hayashi et al. 2004). In humans, this function has been assigned to a complex that comprises three Mis18 homologs Mis18α, Mis18β, and Mis18BP1[HsKNL2] (Fujita et al. 2007); it has been also shown that Mis18BP1[HsKNL2] directly binds CENP-A (Hory et al. 2017; French et al. 2017). It has been proposed that the Mis18 has a histone acetyltransferase activity that modifies chromatin conformation rendering it permissive for CENP-A deposition (Ohzeki et al. 2012, 2016). The chaperone Scm3 in fission yeast and its homolog HJURP in human cells also appear to play a role in CENP-A assembly (Dunleavy et al. 2009; Foltz et al. 2009; Williams et al. 2009). Recently, it has been proposed that also CENP-C and CENP-I are key factors involved in epigenetic maintenance of CENP-A chromatin (Shono et al. 2015).

Most of the components of the vertebrate constitutive centromere-associated network (CCAN) are not conserved in *Drosophila*. While in humans this network is thought to comprise 16 proteins, several studies indicate that *Drosophila* has a single CCAN component, namely, CENP-C (Barth et al. 2014; Chen et al. 2014; Richter et al. 2016). Cid interacts with its loading factor Cal1 and CENP-C to associate with the centromere (Mellone et al. 2011; Chen et al. 2014). Cal1 is not only involved in Cid loading but also prevents excessive incorporation of Cid into the centromeres, which can cause defects in chromosomes segregation (Schittenhelm et al. 2010; Chen et al. 2014).

In this study, we have identified new components of Cid loading machinery.

We have previously found that some Trx-G and Pc-G proteins (e.g., Ph and CBP) localize at the centromeres (Fanti
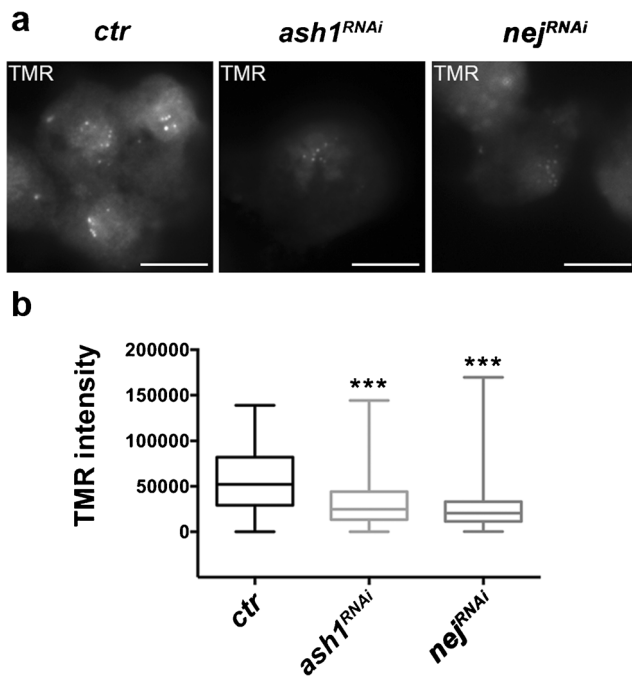
Fig. 9 CBP and Ash1 depletion causes decreased Cid loading. **a** Representative images of interphase SNAP-Cid nuclei showing the recruitment of new SNAP-Cid following the BTP block. TMR-Cid intensity is significantly reduced in *ash1* and *nej* RNAi cells. **b** Quantification of TMR-Cid intensities in *ash1* and *nej* knock-down and control cells. Number of Cid spots analyzed: $n = 196$ for *ctr*, $n = 387$ for *ash1*, and $n = 312$ for *nej*. Statistical significance was determined by ANOVA test ($F = 62.22$, ***$p < 0.001$)

et al. 2008). Here, we have shown that mutations in *trx* and *ash-1* affect chromosome segregation in embryos. We also found that RNAi against *trx*, *ash1*, and *nej* leads to abnormalities in both chromosome structure and segregation without causing defects in the mitotic spindle structure, suggesting a role for these proteins in centromere organization. Our results further indicate these Trx-G proteins localize to the centromeric region of extended chromatin fibers (CRFs). Depletion of Ash1 or CBP and simultaneous depletion of both proteins caused a substantial Cid reduction in the centromeric chromatin, which was detected in both mitotic chromosomes and extended chromatin fibers. In contrast, Trx, Ash1 plus Trx, and CBP plus Trx depletion did not produce a significant decrease in Cid loading in CRFs. Interestingly, simultaneous depletion of both Ash1 and Trx caused an increase in the intensity of Cid signals in mitotic chromosomes detected by immunofluorescence.

Explaining why simultaneous loss of Ash1 and Trx causes an increase in Cid fluorescence at centromeres of mitotic chromosomes but not in Cid association with the CRFs is difficult. We can only speculate about this apparently paradoxical result. It has been proposed that the interspersed blocks of CENP-A/Cid and H3 nucleosomes form a three-dimensional cylindrical structure in mitotic chromosomes, with the H3 nucleosomes prevalently oriented towards the inner of the chromosome and the CENP-A nucleosomes oriented towards the external face, where they can interact with kinetochore proteins (Zheng et al. 2005). It is possible that double Ash1 and Trx depletion alters the three-dimensional conformation of the centromeric chromatin in mitotic chromosomes, promoting the localization of Cid-containing nucleosomes on the outer face of the centromere.

Collectively, the results obtained in the immunostaining and in the quench-chase-pulse labeling experiments strongly suggest that Ash1 and CBP promote Cid deposition at centromeres and that loss of Trx antagonizes the effects of their depletion.

Roles of histone modifications in Cid loading

A long-standing question about the factors that affect chromosome segregation is the role of the epigenetic marks of centromeric histones. Immunofluorescence data on extended chromatin fibers showed that centromeres contain alternating blocks of H3 and CENP-A-containing nucleosomes (Blower et al. 2002). While the amino-terminal tails of the pericentromeric H3 histone contain the K9 methylation repressive mark typical of heterochromatin, centromeric histone H3 blocks are enriched in K4 dimethylation marks, characteristic of active chromatin (Sullivan and Karpen 2004). H3 is poorly acetylated at lysine 9 (Ohzeki et al. 2012), and histone acetylation is generally reduced in centromeric regions, although it was recently shown that histone H4 acetylated at lysine 5 and 12 into the centromere is required for CENP-A deposition in chicken and human cells (Shang et al. 2016). Since the perturbation of histone marks in the centromere of human artificial chromosome (HAC) results in loss of stability and reduced centromeric protein deposition, it has been suggested that H3 acetyl/methyl imbalance can modify the structural organization of centromeric chromatin affecting CENP-A loading (Ohzeki et al. 2012).

Although the Trx and Ash1 proteins interact biochemically and their coding genes interact genetically (Rozovskaia et al. 1999), Trx and Ash1 can form two different complexes, TAC1 and ASH1, in which CBP interact with Trx and Ash1, respectively (reviewed in Grimaud et al. 2006).

These complexes maintain the chromatin in a transcriptionally active state, combining the histone acetylation function of CBP with the methylation functions of Ash1 and Trx. Ash1 has H3K4- and H3K36-specific histone methyltransferase activities (Tanaka et al. 2007; Byrd and Shearn 2003; Dorighi and Tamkun 2013), CBP is a H3K27-specific acetyltransferase (Tie et al. 2009), and Trx monomethylates histone H3K4 and interacts with CBP to promote H3K27 acetylation (Tie et al. 2014). Here, we have shown that the centromeric histone H3 is acetylated in K27 by CBP and that CBP depletion causes both a decrease in H3K27 acetylation and an impairment of Cid loading. This result is consistent with the
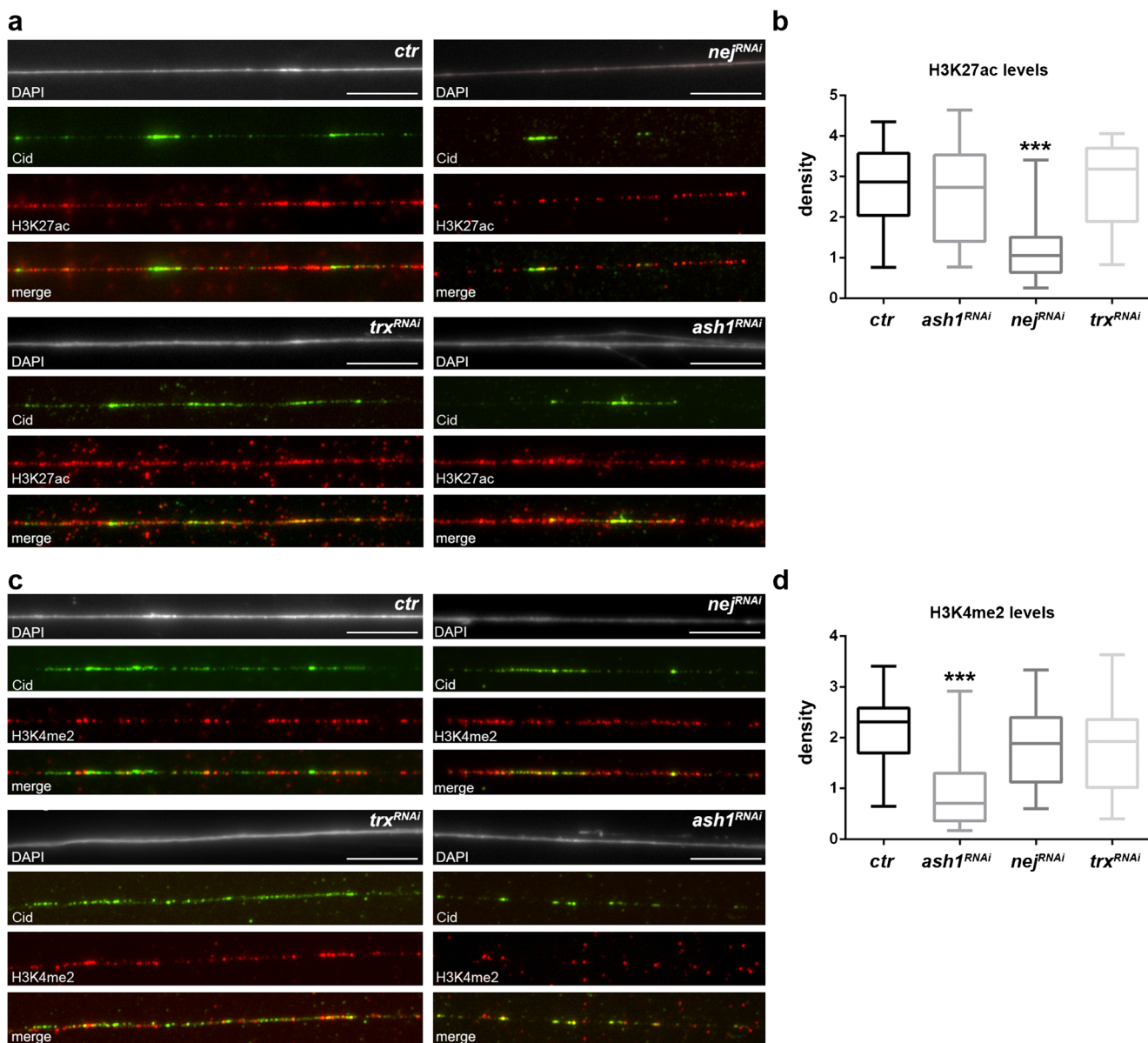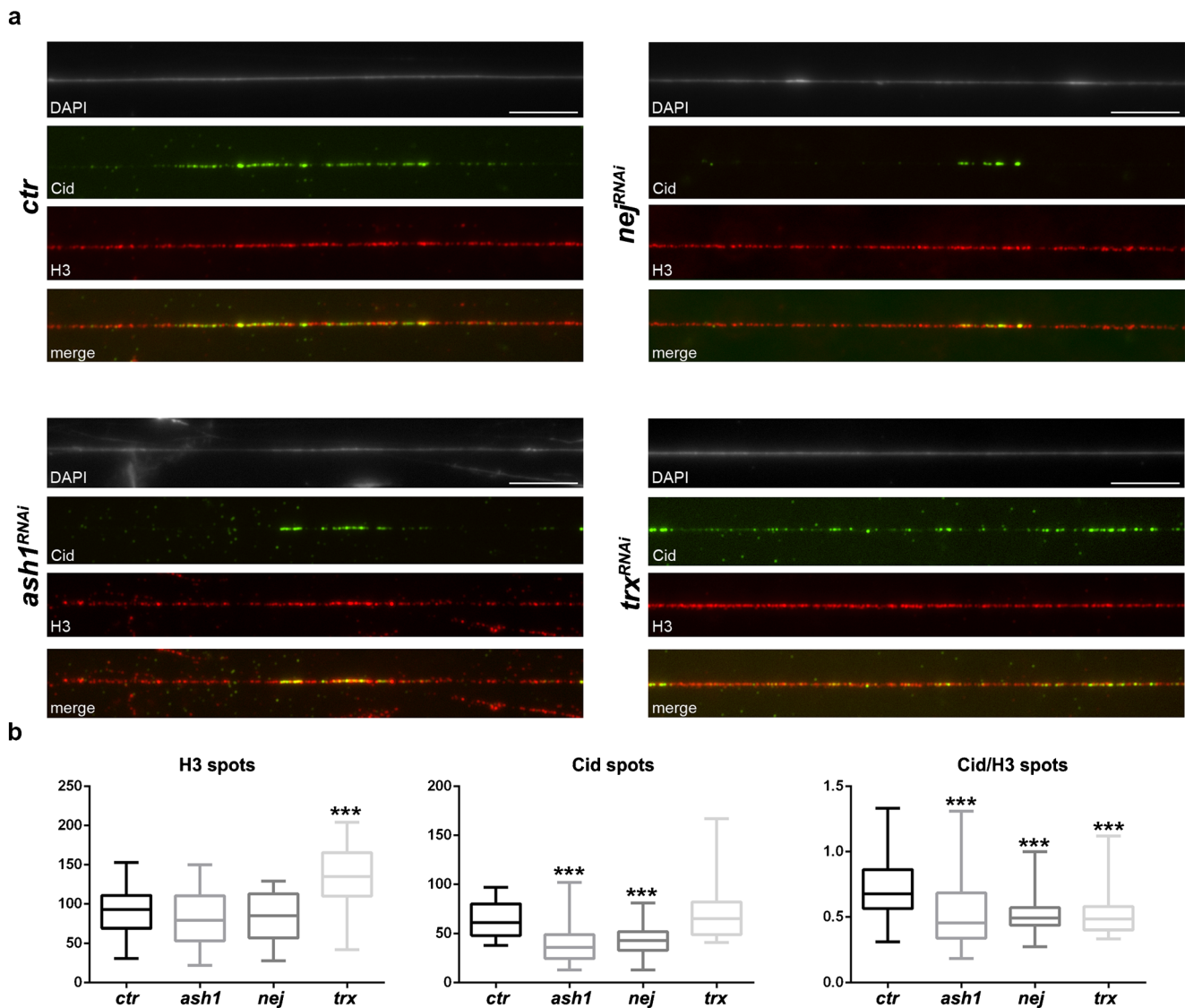
Fig. 10 CBP and Ash1 depletion leads to a decrease in the amount of respectively H3K27ac and H3K4me2 associated with centromeres in extended fibers. **a** Immunostaining of extended fibers from S2 cells with anti-Cid and anti-H3K27ac antibodies. **b** Graphic representation of H3K27ac amount in S2 fibers in which *ash1* ($n = 30$), *nej* ($n = 44$), and *trx* ($n = 27$) are silenced with respect to the control ($n = 40$). **c** Immunostaining of extended fibers from S2 cells with anti-Cid and anti-H3K4me2 antibodies. **d** Graphic representation of H3K4me2 amount in S2 fibers in which *ash1* ($n = 44$), *nej* ($n = 44$), and *trx* ($n = 37$) are silenced with respect to the control ($n = 35$). **a, c** For each panel of *ctr*, *nej^RNAi*, *trx^RNAi*, and *ash1^RNAi*, from the top to bottom: DAPI staining, anti-Cid immunostaining, anti-H3K27ac or anti-H3K4me2 immunostaining, and overlapped images of anti-Cid and anti-H3K27ac or anti-H3K4me2 immunostaining in extended fibers. In **a**, note the different patterns of both Cid and H3K27ac in *nej^RNAi* with respect to the control and to the other fibers. In **c**, note the different patterns of both Cid and H3K4me2 in *ash1^RNAi* with respect to the control and to the other fibers. Scale bar indicates 10 μm. Statistical significance was determined by ANOVA test ($F = 27.15$, ***$p < 0.001$ for H3K27ac density; $F = 21.9$, ***$p < 0.001$ for H3K4me2 density) and Dunnett's multiple comparisons test (***$p < 0.001$).

observation that targeted histone acetyltransferase activity of P300 in HAC is sufficient to induce CENP-A deposition (Ohzeki et al. 2012).

Our results support a model in which the correct CENP-A loading on centromeric chromatin is controlled by post-translational modifications of nucleosomal histones. Current data in *Drosophila* indicate the centromeric histone H3 is di-methylated in lysine 4 (Sullivan and Karpen 2004) and acet-ylated in lysine 27 (as shown here) and that an impairment of these post-translational modifications negatively affects the Cid loading. Thus, these results are consistent with the model of Ohzeki et al. (2012) that proposes that Cid deposition at centromeres requires a correct acetyl/methyl balance. As shown in Fig. 12, when *nej* (CBP) or *ash1* are silenced, the

Fig. 11 Trx depletion increases the amount of H3 histones while CBP and Ash1 depletion do not cause a variation in the amount of H3 histones associated with centromeres in extended fibers. **a** Immunostaining of extended fibers from S2 cells with anti-Cid and anti-H3 antibodies. In **a**, for each panel of *ctr* (n = 33), *nej*[RNAi] (n = 37), *trx*[RNAi] (n = 43), and *ash1*[RNAi] (n = 39), from the top to bottom: DAPI staining, anti-Cid immunostaining, anti-H3 immunostaining, and overlapped images of anti-Cid and anti-H3 in extended fibers. Scale bars indicate 10 μm. **b** Graphic representation of H3 and Cid amount and of the Cid/H3 ratio in S2 fibers in which *ash1*, *nej*, and *trx* are silenced with respect to the control. Statistical significance was determined by ANOVA test (***$p < 0.001$ for H3 spots, $F = 18.91$; ***$p < 0.001$ for Cid spots, F = 19.82; ***$p < 0.001$ for Cid/H3 spots, $F = 7.876$) and Dunnett's multiple comparisons test (***$p < 0.001$)

balance is shifted in favor of H3K4 methylation or H3K27 acetylation, respectively, compromising the correct Cid loading on centromeric chromatin. In contrast, *trx* silencing does not appear to effect the Cid deposition but opposes to the loss of the other two proteins, suggesting that in the absence of Trx, the centromeric chromatin becomes more permissive to Cid incorporation. Because H3K4me2 and H3K27ac are both active chromatin markers, our results also suggest a different scenario, not necessarily alternative to the histone acetyl/methyl balance model, based on a minimal concentration of active marks needed for Cid deposition. It is indeed possible that loss of active epigenetic marks below a certain threshold

could induce chromatin conformational changes making the centromeric chromatin more compact and non-permissive for Cid deposition. This scenario is also partially supported by the recent results of Molina et al. (2016, 2017) that show the failure of H4K12ac, but not of H3K9ac, to rescue the CENP-A deposition after H3K4me2 removal in human cells. It could be hypothesized that the Trx depletion counteracts this state of chromatin compaction, thereby favoring Cid deposition. Instead, the result that H3 histones increase when Trx is depleted seems to contradict this point of view. Trx protein has the function of opening the chromatin, and when depleted, the greater compaction of the centromeric chromatin does not

CID loading nucleosomes   ■ H3K27ac

H3 loading nucleosomes   ● H3K4me2
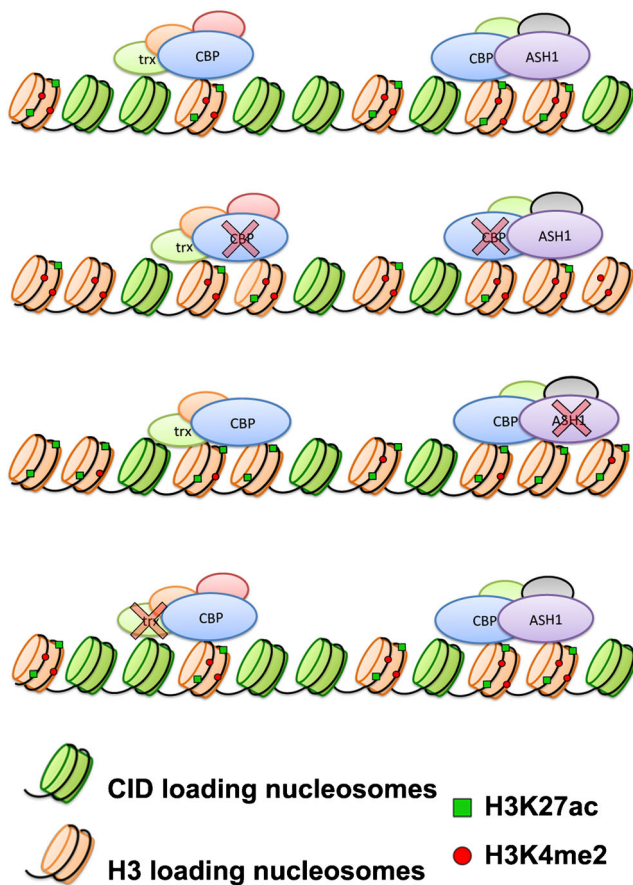
Fig. 12 Schematic representation of the functional role of Ash1, CBP, and Trx proteins in the centromeric region. These proteins act modifying the epigenetic state of the centromeric chromatin. The correct acetyl/methyl balance and/or the correct active mark amount in the interspersed histone H3 nucleosomes determines an active state of the chromatin which, in turn, favors the Cid deposition. When acetylation or methylation are affected by respectively *nej* and *ash1* silencing, the changed chromatin state causes a Cid loading decrease. *trx* silencing does not affect the Cid loading because this protein probably supports and/or antagonizes both Ash1 and CBP in their function and therefore does not affect the acetylation and methylation levels. Note that in this scheme, we want to represent the amount and the localization of the histone modifications and not the level of chromatin compaction

affect the Cid loading, since the necessary epigenetic marks are present.

It is currently unclear whether the epigenetic landscape of the centromeric regions directly permits Cid deposition or is instead necessary for transcriptional activation of centromeric sequences, which in turn regulates the Cid deposition. Over the last few years, active transcription of centromeric sequences has been observed in several organisms (Bergmann et al. 2011; Choi et al. 2011; Chan et al. 2012; Quenet and Dalal 2014; McNulty et al. 2017) including *Drosophila* (Rošić et al. 2014; Chen et al. 2015; Bobkov et al. 2018). Non-coding transcripts from the 359-bp satellite DNA (Sat III) associate with all *Drosophila* major chromosomes and are required for the correct localization of CENP-C and Cid (Rošić et al.

2014). More recently, Bobkov et al. (2018) found that RNA polymerase II localizes to *Drosophila* centromeres and that Cid deposition coincides with RNA polymerase activity at centromeres.

In conclusion, this study clearly shows that both *ash1* and *nej* (CBP) are required for correct localization of Cid at *Drosophila* centromeres. Our data also suggest that these genes control Cid deposition through histone post-translational modifications. However, the precise underlying mechanism through which these modifications regulate Cid recruitment remains to be defined.

Compliance with ethical standards

References

Ahmad K, Henikoff S (2001) Centromeres are specialized replication domains in heterochromatin. J Cell Biol 153:101–110

Amor DJ, Kalitsis P, Sumer H, Choo KH (2004) Building the centromere: from foundation proteins to 3D organization. Trends Cell Biol 14:359–368

Barth TK, Schade GO, Schmidt A, Vetter I, Wirth M, Heun P, Thomae AW, Imhof A (2014) Identification of novel *Drosophila* centromere-associated proteins. Proteomics 14:2167–2178

Baum M, Sanyal K, Mishra PK, Thaler N, Carbon J (2006) Formation of functional centromeric chromatin is specified epigenetically in *Candida albicans*. Proc Natl Acad Sci U S A 103:14877–14882

Bergmann JH, Rodríguez MG, Martins NM, Kimura H, Kelly DA, Masumoto H, Larionov V, Jansen LE, Earnshaw WC (2011) Epigenetic engineering shows H3K4me2 is required for HJURP targeting and CENP-A assembly on a synthetic human kinetochore. EMBO J 30:328–340

Bernad R, Sánchez P, Losada A (2009) Epigenetic specification of centromeres by CENP-A. Exp Cell Res 315:3233–3241

Bhat KM, Farkas G, Karch F, Gyurkovics H, Gausz J, Schedl P (1996) The GAGA factor is required in the early *Drosophila* embryo not only for transcriptional regulation but also for nuclear division. Development 122:1113–1124

Blower MD, Karpen GH (2001) The role of *Drosophila* CID in kinetochore formation, cell-cycle progression and heterochromatin interactions. Nat Cell Biol 3:730–739

Blower MD, Sullivan BA, Karpen GH (2002) Conserved organization of centromeric chromatin in flies and humans. Dev Cell 2:319–330

Bobkov GOM, Gilbert N, Heun P (2018) Centromere transcription allows CENP-A to transit from chromatin association to stable incorporation. J Cell Biol 217:1957–1972

Boltengagen M, Huang A, Boltengagen A, Trixl L, Lindner H, Kremser L, Offterdinger M, Lusser A (2016) A novel role for the histone acetyltransferase Hat1 in the CENP-A/CID assembly pathway in Drosophila melanogaster. Nucleic Acids Res 44:2145–2159

Buchwitz BJ, Ahmad K, Moore LL, Roth MB, Henikoff S (1999) A histone-H3-like protein in C. elegans. Nature 401:547–548

Byrd KN, Shearn A (2003) ASH1, a Drosophila Trithorax group protein, is required for methylation of lysine 4 residues on histone H3. Proc Natl Acad Sci U S A 100:11535–11540

Chan FL, Marshall OJ, Saffery R, Kim BW, Earle E, Choo KH, Wong LH (2012) Active transcription and essential role of RNA polymerase II at the centromere during mitosis. Proc Natl Acad Sci U S A 109:1979–1984

Chen C, Mellone BG (2016) Chromatin assembly: journey to the CENter of the chromosome. JCB 214:13–24

Chen CC, Dechassa ML, Bettini E, Ledoux MB, Belisario C, Heun P, Luger K, Mellone BG (2014) Cal1 is the Drosophila CENP-A assembly factor. J Cell Biol 204:313–329

Chen CC, Bowers S, Lipinszki Z, Palladino J, Trusiak S, Bettini E, Rosin L, Przewloka MR, Glover DM, O'Neill RJ, Mellone BG (2015) Establishment of centromeric chromatin by the CENP-A assembly factor CAL1 requires FACT-mediated transcription. Dev Cell 34:73–84

Choi S, Kim W, Chung J (2011) Drosophila salt-inducible kinase (SIK) regulates starvation resistance through cAMP-response element-binding protein (CREB)-regulated transcription coactivator (CRTC). J Biol Chem 286:2658–2664

Craig JM, Earle E, Canham P, Wong LH, Anderson M, Choo KH (2003) Analysis of mammalian proteins involved in chromatin modification reveals new metaphase centromeric proteins and distinct chromosomal distribution patterns. Human Mol Genet 12:3109–3121

De Rop V, Padeganeh A, Maddox PS (2012) CENP-A: the key player behind centromere identity, propagation, and kinetochore assembly. Chromosoma 121:527–538

Dorighi KM, Tamkun JW (2013) The trithorax group proteins Kismet and ASH1 promote H3K36 dimethylation to counteract Polycomb group repression in Drosophila. Development 140:4182–4192

du Sart D, Cancilla MR, Earle E, Mao JI, Saffery R, Tainton KM, Kalitsis P, Martyn J, Barry AE, Choo KH (1997) A functional neo-centromere formed through activation of a latent human centromere and consisting of non-alpha-satellite DNA. Nat Genet 16:144–153

Dunleavy EM, Roche D, Tagami H, Lacoste N, Ray-Gallet D, Nakamura Y, Daigo Y, Nakatani Y, Almouzni-Pettinotti G (2009) HJURP is a cell-cycle-dependent maintenance and deposition factor of CENP-A at centromeres. Cell. 137:485–497

Earnshaw WC, Rothfield N (1985) Identification of a family of human centromere proteins using autoimmune sera from patients with scleroderma. Chromosoma 91:313–321

Ekwall K (2007) Epigenetic control of centromere behavior. Annu Rev Genet 41:63–81

Fanti L, Pimpinelli S (2004) Immunostaining of squash preparations of chromosomes of larval brains. In Drosophila Cytogentics Protocols. Methods Mol Biol 247:353–361. Edited by DS. Henderson. Humana Press Inc.

Fanti L, Perrini B, Piacentini L, Berloco M, Marchetti E, Palumbo G, Pimpinelli S (2008) The trithorax group and Pc group proteins are differentially involved in heterochromatin formation in Drosophila. Chromosoma 117:25–39

Foltz DR, Jansen LE, Bailey AO, Yates JR 3rd, Bassett EA, Wood S, Black BE, Cleveland DW (2009) Centromere-specific assembly of CENP-a nucleosomes is mediated by HJURP. Cell 137:472484

French BT, Westhorpe FG, Limouse C, Straight AF (2017) Xenopus laevis M18BP1 directly binds existing CENP-A nucleosomes to promote centromeric chromatin assembly. Dev Cell 42:190–199

Fujita Y, Hayashi T, Kiyomitsu T, Toyoda Y, Kokubu A, Obuse C, Yanagida M (2007) Priming of centromere for CENP-A recruitment

by human hMis18alpha, hMis18beta, and M18BP1. Dev Cell 12:17–30

Fukagawa T, Earnshaw WC (2014) The centromere: chromatin foundation for the kinetochore machinery. Dev Cell 30:496–508

Geisler SJ, Paro R (2015) Trithorax and Polycomb group-dependent regulation: a tale of opposing activities. Development 142:2876–2887

Grimaud C, Nègre N, Cavalli G (2006) From genetics to epigenetics: the tale of Polycomb group and trithorax group genes. Chromosome Res 14:363-375. Review. Erratum in: Chromosome Res 14(6):701

Hayashi T, Fujita Y, Iwasaki O, Adachi Y, Takahashi K, Yanagida M (2004) Mis16 and Mis18 are required for CENP-A loading and histone deacetylation at centromeres. Cell 118:715–729

Hory T, Shang WH, Hara M, Ariyoshi M, Arimura Y, Fujita R, Kurumizaka H, Fukagawa T (2017) Association of M18BP1/KNL2 with CENP-A nucleosome is essential for centromere formation in non-mammalian vertebrate. Dev Cell 42:181–189

Howman EV, Fowler KJ, Newson AJ, Redward S, MacDonald AC, Kalitsis P, Choo KH (2000) Early disruption of centromeric chromatin organization in centromere protein A (Cenpa) null mice. Proc Natl Acad Sci U S A 97:1148–1153

Jansen LE, Black BE, Foltz DR, Cleveland DW (2007) Propagation of centromeric chromatin requires exit from mitosis. J Cell Biol 176:795–805

Kennison JA (1993) Transcriptional activation of Drosophila homeotic genes from distant regulatory elements. Trends Genet 9:75–79

Lidsky PV, Sprenger F, Lehner CF (2013) Distinct modes of centromere protein dynamics during cell cycle progression in Drosophila S2R+ cells. J Cell Sci 126:4782–4793

Lupo R, Breiling A, Bianchi ME, Orlando V (2001) Drosophila chromosome condensation proteins topoisomerase II and barren colocalize with Polycomb and maintain Fab-7 PRE silencing. Mol Cell 7:127–136

McKinley LM, Cheeseman IM (2016) The molecular basis for centromere identity and function. Nat Rev Mol Cell Biol 17:16–29

McNulty SM, Sullivan LL, Sullivan BA (2017) Human centromeres produce chromosome-specific and array-specific alpha satellite transcripts that are complexed with CENP-A and CENP-C. Dev Cell 42:226–240

Mellone BG, Grive KJ, Shteyn V, Bowers SR, Oderberg I, Karpen GH (2011) Assembly of Drosophila centromeric chromatin proteins during mitosis. PLoS Genet 7:e1002068. https://doi.org/10.1371/journal.pgen.1002068

Meluh PB, Strunnikov AV (2002) Beyond the ABCs of CKC and SCC. Do centromeres sister chromatid cohesion or viceversa? The FEBS journal 269:2300–2314

Molina O, Vargiu G, Abad MA, Zhiteneva A, Jeyaprakash AA, Masumoto H, Kouprina N, Larionov V, Earnshaw WC (2016) Epigenetic engineering reveals a balance between histone modifications and transcription in kinetochore maintenance. Nature Comm 7:13334

Molina O, Kouprina N, Masumoto H, Larionov V, Earnshaw WC (2017) Using human artificial chromosomes to study centromere assembly and function. Chromosoma 126:559–575

Muller S, Almouzni G (2017) Chromatin dynamics during the cell cycle at centromeres. Nat Rev Genet 18:192–208

Naito Y, Yamada T, Matsumiya T, Ui-Tei K, Saigo K, Morishita S (2005) dsCheck: highly sensitive off-target search software for double-stranded RNA-mediated RNA interference. Nucleic Acids Res 33(Web Server issue):W589–W591

Nakano M, Cardinale S, Noskov VN, Gassmann R, Vagnarelli P, Kandels-Lewis S, Larionov V, Earnshaw WC, Masumoto H (2008) Inactivation of a human kinetochore by specific targeting of chromatin modifiers. Dev Cell 14:507–522

Oegema K, Desai A, Rybina S, Kirkham M, Hyman A (2001) Functional analysis of kinetochore assembly in Caenorhabditis elegans. J Cell Biol 153:1209–1226

Ohzeki J, Bergmann JH, Kouprina N, Noskov VN, Nakano M, Kimura H, Earnshaw WC, Larionov V, Masumoto H (2012) Breaking the HAC barrier: histone H3K9 acetyl/methyl balance regulates CENP-A assembly. EMBO J 31:2391–2402

Ohzeki J, Shono N, Otake K, Martins NMC, Kogou K, Kimura H, Nagase T, Larionov V, Earnshaw WC, Masumoto H (2016) KAT7/HBOI/MYST2 regulates CENP-A chromatin assembly by antagonizing Suv39h1-mediated centromere inactivation. Dev Cell 37:413–427

Petruk S, Sedkov Y, Smith S, Tillib S, Kraevski V, Nakamura T, Canaani E, Croce CM, Mazo A (2001) Trithorax and dCBP acting in a complex to maintain expression of a homeotic gene. Science 294: 1331–1334

Przewloka MR, Glover DM (2009) The kinetochore and the centromere: a working long distance relationship. Annu Rev Genet 43:439–465

Quenet D, Dalal Y (2014) A long non-coding RNA is required for targeting centromeric protein A to the human centromere. eLife 3: e03254

Régnier V, Vagnarelli P, Fukagawa T, Zerjal T, Burns E, Trouche D, Earnshaw W, Brown W (2005) CENP-A is required for accurate chromosome segregation and sustained kinetochore association of BubR1. Mol Cell Biol 25:3967–3981

Richter MM, Poznanski J, Zdziarska A, Czarnocki-cieciura M, Lipinski Z, Dadlez M, Glover DM, Przewloka MR (2016) Network of protein interactions within the *Drosophila* inner kinetochore. Open Biol 6(2):150238

Rošić S, Ehardt S (2016) No longer a nuisance: long non-coding RNAs join CENP-A in epigenetic centromere regulation. Cell Mol Life Sci 73:1387–1398

Rošić S, Köhler F, Erhardt S (2014) Repetitive centromeric satellite RNA is essential for kinetochore formation and cell division. J Cell Biol 207:335–349

Rothwell WF, Sullivan W (1999) Fluorescent analysis of *Drosophila* embryos. In: Sullivan, Ashburner, Hawley (eds) Drosophila Protocols. Cold Spring Harbor laboratory Press, pp 141–157

Rozenblatt-Rosen O, Rozovskaia T, Burakov D, Sedkov Y, Tillib S, Blechman J, Nakamura T, Croce CM, Mazo A, Canaani E (1998) The C-terminal SET domains of ALL-1 and TRITHORAX interact with the INI1 and SNR1 proteins, components of the SWI/SNF complex. Proc Natl Acad Sci U S A 95:4152–4157

Rozovskaia T, Tillib S, Smith S, Sedkov Y, Rozenblatt-Rosen O, Petruk S, Yano T, Nakamura T, Ben-Simchon L, Gildea J, Croce CM, Shearn A, Canaani E, Mazo A (1999) Trithorax and ASH1 interact directly and associate with the trithorax group-responsive bxd region of the Ultrabithorax promoter. Mol Cell Biol 19:6441–6447

Schittenhelm RB, Althoff F, Heidmann S, Lehner CF (2010) Detrimental incorporation of excess Cenp-A/Cid and Cenp-C into *Drosophila* centromeres is prevented by limiting amounts of the bridging factor Cal1. J Cell Sci 123:3768–3779

Schneider I (1972) Cell lines derived from late embryonic stages of *Drosophila melanogaster*. J Embryol exp Morphol 27:353–365

Schuh M, Lehner CF, Heidmann S (2007) Incorporation of *Drosophila* CID/CENP-A and CENP-C into centromeres during early embryonic anaphase. Curr Biol 17:237–243

Shang WH, Hori T, Westhorpe FG, Godek KM, Toyoda A, Misu S, Monma N, Ikeo K, Carroll CW, Takami Y, Fujiyama A, Kimura H, Straight AF, Fukagawa T (2016) Acetylation of histone H4 lysine 5 and 12 is required for CENP-A deposition into centromeres. Nat Commun 7:13465

Shono N, Ohzeki J, Otake K, Martins NM, Nagase T, Kimura H, Larionov V, Earnshaw WC, Masumoto H (2015) CENP-C and CENP-I are key connecting factors for kinetochore and CENP-A assembly. J Cell Sci 128:4572–4587

Smolik S, Jones K (2007) *Drosophila* dCBP is involved in establishing the DNA replication checkpoint. Mol Cell Biol 27:135–146

Somma MP, Ceprani F, Bucciarelli E, Naim V, De Arcangelis V, Piergentili R, Palena A, Ciapponi L, Giansanti MG, Pellacani C, Petrucci R, Cenci G, Vernì F, Fasulo B, Goldberg ML, Di Cunto F, Gatti M (2008) Identification of *Drosophila* mitotic genes by combining co-expression analysis and RNA interference. PLoS Genet 4:e1000126

Sullivan BA, Karpen GH (2004) Centromeric chromatin exhibits a histone modification pattern that is distinct from both euchromatin and heterochromatin. Nat Struct Mol Biol 11:1076–1083

Sullivan KF, Hechenberger M, Masri K (1994) Human CENP-A contains a histone H3 related histone fold domain that is required for targeting to the centromere. J Cell Biol 127:581–592

Takahashi K, Chen ES, Yanagida M (2000) Requirement of Mis6 centromere connector for localizing a CENP-A-like protein in fission yeast. Science 288:2215–2219

Tanaka Y, Katagiri Z, Kawahashi K, Kioussis D, Kitajima S (2007) Trithorax-group ASH1 methtlates histone H3 lysine 36. Gene 397: 161–168

Tie F, Banerjee R, Stratton CA, Prasad-Sinha J, Stepanik V, Zlobin A, Diaz MO, Scacheri PC, Harte PJ (2009) CBP-mediated acetylation of histone H3 lysine 27 antagonizes *Drosophila* Polycomb silencing. Development. 136:3131–3141

Tie F, Banerjee R, Saiakhova AR, Howard B, Monteith KE, Scacheri PC, Cosgrove MS, Harte PJ (2014) Trithorax monomethylates histone H3K4 and interacts directly with CBP to promote H3K27 acetylation and antagonize Polycomb silencing. Development. 141:1129–1139

Tripoulas N, LaJeunesse D, Gildea J, Shearn A (1996) The *Drosophila ash1* gene product, which is localized at specific sites on polytene chromosomes, contains a SET domain and a PHD finger. Genetics 143:913–928

Ui K, Nishihara S, Sakuma M, Togashi S, Ueda R, Miyata Y, Miyake T (1994) Newly established cell lines from *Drosophila* larval CNS express neural specific characteristics. In Vitro Cell Dev Biol Anim 30:209–216

Voullaire LE, Slater HR, Petrovic V, Choo KH (1993) A functional marker centromere with no detectable alpha-satellite, satellite III, or CENP-B protein: activation of a latent centromere? Am J Hum Genet 52:1153–1163

Warburton PE (2004) Chromosomal dynamics of human neocentromere formation. Chromosom Res 12:617–626

Warburton PE, Cooke CA, Bourassa S, Vafa O, Sullivan BA, Stetten G, Gimelli G, Warburton D, Tyler-Smith C, Sullivan KF, Poirier GG, Earnshaw WC (1997) Immunolocalization of CENP-A suggests a distinct nucleosome structure at the inner kinetochore plate of active centromeres. Curr Biol:7901–7904

Williams JS, Hayashi T, Yanagida M, Russell P (2009) Fission yeast Scm3 mediates stable assembly of Cnp1/CENP-A into centromeric chromatin. Mol Cell 33:287–298

Zheng C, Lu X, Hansen JC, Hayes JJ (2005) Salt-dependent intra- and internucleosomal interactions of the H3 tail domain in a model oligonucleosomal array. J Biol Chem 280:33552–33557